

Thermal Decomposition Mechanisms of Volatile Molybdenum(VI) Bis-Imides

Michael A. Land,^{*[a]} Goran Bačić,^[a] Katherine N. Robertson,^[b] and Seán T. Barry^[a]

[a] Department of Chemistry, Carleton University, 1125 Colonel By Drive, Ottawa, Ontario, K1S 5B6 Canada.

[b] Department of Chemistry, Saint Mary's University, 923 Robie Street, Halifax, Nova Scotia, B3H 3C3 Canada.

Thermal Stability, Thermolysis, Vapor Deposition, Mechanism, Molybdenum

Abstract

The bis(*tert*-butylimido)-molybdenum(VI) framework has been used successfully in the design of vapor-phase precursors for molybdenum-containing thin films, so understanding its thermal behavior is important for such applications. Here we report the thermal decomposition mechanism for a series of volatile bis(alkylimido)-dichloromolybdenum(VI) adducts with neutral *N,N'*-chelating ligands, to probe the stability and decomposition pathways for these industrially relevant molecules. The alkyl groups explored were *tert*-butyl, *tert*-pentyl, 1-adamantyl, and a cyclic imido (from 2,5-dimethylhexane-2,5-diamine). We also report the synthesis of the new *tert*-octyl imido adducts, (^tOctN)₂MoCl₂·L (L = *N,N,N',N'*-tetramethylethylenediamine or 2,2'-bipyridine), which

have been fully characterized by spectroscopic techniques as well as single-crystal X-ray diffraction and thermal analysis. We found that the decomposition of all compounds follows the same general pathway, proceeding first by the dissociation of the chelating ligand to give the coordinatively unsaturated species $(\text{RN})_2\text{MoCl}_2$. Subsequent dimerization results in either an imido bridged adduct, $[(\text{RN})\text{Mo}(\mu\text{-NR})\text{Cl}_2]_2$, or a chloride bridged adduct, $[(\text{RN})_2\text{Mo}(\mu\text{-Cl})\text{Cl}]_2$, depending on the size of the R group. The dimeric species then undergoes an intramolecular γ -hydrogen transfer to yield a nitrido-amido adduct, $(\text{RHN})\text{MoNCl}_2$, and an alkene. Ultimately, the resulting molybdenum species decomposes into free *tert*-alkylamine and $\beta\text{-Mo}_2\text{N}$. The thermolysis reactions have been monitored using ^1H NMR spectroscopy, and the volatile decomposition products were analyzed using gas chromatography–mass spectrometry. A key intermediate has also been detected using electron ionization high-resolution mass spectrometry. Finally, a detailed computational investigation supports the mechanism outlined above and helps explain the relative stabilities of different *N,N'*-chelated bis(alkylimido)-dichloromolybdenum(VI) adducts.

Introduction

Molybdenum(VI) bis(imido) compounds have a wide range of applications, including their use as olefin metathesis catalysts,^{1,2} oxygen atom transfer reagents,^{3–6} and vapor phase deposition precursors.^{7–42} The reactivity of these industrially relevant compounds has been extensively studied, but the mechanism of their thermal decomposition remains poorly understood. Both the temperature at which and the mechanism by which a compound decomposes must be understood so that the primary decomposition pathways can be blocked effectively through ligand and complex design to enhance thermal stability.^{43–47} Understanding the thermal decomposition of compounds is particularly relevant to chemical vapor deposition (CVD) and atomic layer

deposition (ALD).⁴⁸ In both deposition methods, precursors are vaporized and delivered to a substrate where they undergo gas-surface reactions to continuously grow thin films (by CVD) or self-limiting monolayers (by ALD). Understanding how these precursors decompose can also provide information on the composition of a film grown using a compound as a single-source precursor (for CVD) or the upper temperature limits of thermal stability (for ALD).⁴⁹

The bis(*tert*-butylimido)molybdenum(VI) framework has been used for the deposition of various molybdenum-containing films. For example, various anionic ligands have been explored, resulting in varying thermal properties and surface reactivities (Chart 1). Specifically, amido (**A** and **B**),^{8,19,24} amidinate (**C**),^{9,10} guanidinate (**D**),⁴¹ and chloro (**E**)⁷ compounds have been used for the CVD of MoN_x or MoC_xN_y, and amidinate (**C**),¹⁸ diazabutadienyl (**F**),³¹ and thiolate (**G**)²⁹ compounds have been used for the CVD of MoS₂. Additionally, MoN_x nanoparticles have been obtained by thermolysis of the pyrazolate (**H**).³⁰ Interestingly, this class of compound has not been used for the CVD of MoO₃ or MoON, possibly due to the inherent strength of the Mo=N bond. However, molybdenum oxide films have been prepared using these precursors with ALD methods in conjunction with O₃ or O₂ plasma, which is able to disrupt the strong Mo=N bond. For example, the amide **A**^{11,14} and the amidinate **C**²⁰ have been used to prepare MoO₃ thin films by ALD. The amide **A** has also been used as a precursor for the ALD of MoN_x,^{37,38} MoS₂,^{21,25,26} MoC_xN_y,^{16,24} Al:MoS₂,³² and TiMo_xN_y.³⁴ Finally, the thiolate **G** has also been used for the ALD of Mo₂N films with H₂ plasma.¹⁵

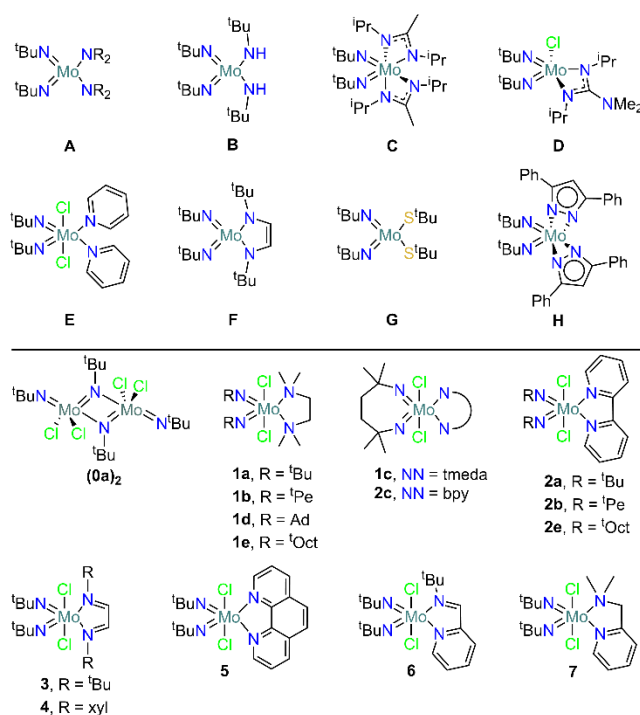


Chart 1. Known CVD and ALD precursors (**A-H**) that incorporate the bis(*tert*-butylimido)molybdenum(VI) framework and the general $(\text{RN})_2\text{MoCl}_2\cdot\text{L}$ (L = neutral N,N' -chelating ligand) compounds (**1-7**). R = Me, Et, ⁱPr; ^tBu = *tert*-butyl; ^tPe = *tert*-pentyl; Ad = 1-adamantyl; ^tOct = *tert*-octyl; xyl = 2,6-dimethylphenyl.

Despite these compounds having been used as deposition precursors, only preliminary studies have been performed on their thermal stabilities and decomposition mechanisms. Winter *et al.* proposed that both *tert*-butyl imido groups in the pyrazolate **H** initially undergo γ -H elimination resulting in hydrogen-terminated imido groups, with the elimination of isobutylene.³⁰ Fischer *et al.* have proposed that the amidinate ligands (in **C**) decompose *via* γ -H elimination of the imido groups, subsequently resulting in hydrogen-terminated imido groups, on the basis of electron ionization mass spectrometry (EI-MS) fragmentation analysis.⁹ Additionally, Pakkanen *et al.* have proposed several decomposition routes in the amido adducts **A**, due to the presence of β -H or β -

methyl groups (in the NR_2 ligands); these decompositions were found to be endergonic with enthalpies between 35.1 and 11.3 $\text{kcal}\cdot\text{mol}^{-1}$ using DFT (B3LYP/LANL2DZ), but the reaction mechanism was not explored.³⁸ Recently, McElwee-White *et al.* have studied the decomposition of the thiolate compound **G**, and found isobutylene and *tert*-butylamine to be the primary decomposition products (using GC-MS and ^1H NMR spectroscopy), resulting in compounds containing either a terminal nitrido ($\text{Mo}\equiv\text{N}$) or sulfido ($\text{Mo}=\text{S}$) group.²⁹ Finally, the mechanism of isobutylene elimination from the tungsten analogue of **A**, $(^t\text{BuN})_2\text{W}(\text{NMe}_2)_2$, was investigated computationally,⁵⁰ an activation barrier of 69.7 kcal mol^{-1} , for the γ -H elimination resulting in the formation of isobutylene and a hydrogen-terminated imido, was found in the absence of a co-reagent (i.e., acting as a single-source precursor).⁵⁰ While this barrier can be overcome under CVD conditions at high temperatures and through surface-catalyzed reactions, it does not correlate with the solid-state thermolysis temperatures for these compounds ($T_{\text{D}} = 190$ °C for $(^t\text{BuN})_2\text{Mo}(\text{NMe}_2)_2$ and 310 °C for $(^t\text{BuN})_2\text{W}(\text{NMe}_2)_2$).⁵¹ Given the inconclusive nature of this set of studies, we set out to clarify a mechanism for the thermolysis of a series of bis(alkylimido)-dichloromolybdenum(VI) complexes (Chart 1).

We recently reported an experimental investigation of the role of various alkyl groups and *N,N'*-chelates on the volatility and thermal stability of such Mo(VI) complexes.³⁶ The 1,4-di-*tert*-butyl-1,3-diazabutadiene adduct, $(^t\text{BuN})_2\text{MoCl}_2\cdot^t\text{Bu}^t\text{dad}$ (**3**) was found to be the most volatile compound, achieving 1 Torr of vapor pressure (T_{V}) at 135 °C,³⁶ and the 1,10-phenanthroline adduct, $(^t\text{BuN})_2\text{MoCl}_2\cdot\text{phen}$ (**5**), was found to be the most thermally stable, with an onset of decomposition (T_{D}) of 303 °C, but at the cost of reduced volatility. Additionally, we found that we could use “hybrid” ligands, such as *tert*-butyl(pyridine-2-yl-methyleneamine) to prepare $(^t\text{BuN})_2\text{MoCl}_2\cdot\text{impy}$ (**6**), which combined the volatility of the $^t\text{Bu}^t\text{dad}$ adduct with the thermal

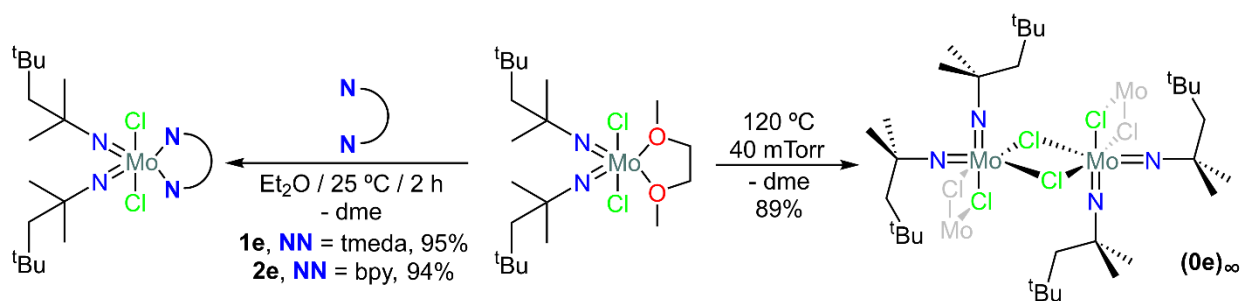
stability of the bpy adduct. While we could tune the volatility and stability of the precursors, the details of the decomposition mechanism remained unexplored; a deeper understanding of the mechanism(s) is crucial for the continued design of new and better precursors. Here we report the results from a combined experimental and computational investigation into the thermal decomposition of bis(alkylimido)-dichloromolybdenum(VI) complexes.

Results and Discussion

Synthesis and Characterization

The alkyl groups on the imido ligands in the series in Chart 1 are *tert*-butyl, *tert*-pentyl, 1-adamantyl, and a cyclic imido (from 2,5-dimethylhexane-2,5-diamine), all of which contain a quaternary carbon atom bound to the imido group; they are thus expected to follow similar decomposition pathways. For this study, we also prepared the *tert*-octyl derivative to further probe the decomposition mechanism, as the alkenes expected from the thermolysis of this compound would be easy to handle and subsequently detect. The synthesis of the bis(*tert*-octyl)imido-dichloromolybdenum(VI) 1,2-dimethoxyethane (dme) adduct had previously been described in a patent,⁵² but without characterization data. We prepared (^tOctN)MoCl₂·dme from Na₂MoO₄ following a slightly modified literature procedure (see the experimental section),⁵² then treated it with *N,N,N',N'*-tetramethylethylenediamine (tmeda) or 2,2'-bipyridine (bpy) to form (^tOctN)MoCl₂·tmeda (**1e**) and (^tOctN)MoCl₂·bpy (**2e**), respectively, with excellent yields (Scheme 1). As expected, the ¹H NMR spectra of both **1e** and **2e** revealed equivalent *tert*-octyl environments; other chemical shifts were as expected and well resolved. Thermogravimetric analysis (TGA) of the *tert*-octyl compounds (Figures S50 and S51) revealed both to be more volatile than their *tert*-butyl analogues (**1a** and **2a**), achieving *T_v* at 140 and 205 °C for **1e** and **2e**

respectively (compared to the T_v for **1a** at 173 °C and **2a** at 249 °C).³⁶ Despite both compounds exhibiting relatively good volatilities, high residual masses of 22% and 19%, respectively, were observed in the TGA. The high residual masses correlate with poor thermal stability, compared to the *tert*-butyl analogues, as shown by differential scanning calorimetry (DSC, Figures S54 and S55); the T_D for **1e** and **2e** were 154 and 226 °C, respectively.



Scheme 1. Synthesis of the $({}^t\text{OctN})_2\text{MoCl}_2$ adducts (**1e** and **2e**) and the polymeric compound $[({}^t\text{OctN})_2\text{MoCl}(\mu\text{-Cl})_2]_\infty$ (**0e**) $_\infty$. The gray-colored atoms show how the dimeric unit extends into polymeric chains.

We had previously studied the volatility of $({}^t\text{BuN})_2\text{MoCl}_2 \cdot \text{dme}$ and found it to readily liberate *dme* upon heating, resulting in the formation of a bridging imido dimer, $[({}^t\text{BuN})\text{Mo}(\mu\text{-N}{}^t\text{Bu})\text{Cl}_2]_2$ (**0a**)₂.²⁸ Therefore, we performed the analogous experiment with $({}^t\text{OctN})_2\text{MoCl}_2 \cdot \text{dme}$ and after sublimation an orange solid was isolated in high yield (Scheme 1). Single-crystal X-ray crystallography showed the structure to be a coordination polymer comprised of bridging chloride dimeric units, $[({}^t\text{OctN})_2\text{Mo}(\mu\text{-Cl})_2]_\infty$ (**0e**) $_\infty$ (further discussed below). ¹H and ¹³C NMR spectroscopy revealed only a single *tert*-octyl environment, suggesting that the chloride bridge may be maintained in the solution phase; asymmetry would be observed if the dimer bridged through the imide. TGA of $({}^t\text{OctN})_2\text{MoCl}_2 \cdot \text{dme}$ clearly showed the loss of *dme* after which the

remaining mass-loss curve resembled the TGA of **(0e)**_∞, both of which resulted in a high residual mass (Figures S52 and S53). Like the other *tert*-octyl adducts (**1e** and **2e**) the high residual mass likely results from decomposition before evaporation is complete. Clearly, the *tert*-octyl compounds are not ideal vapor deposition precursor candidates, however, their similarities to the other compounds in this series made them a valuable addition to this exploration of decomposition mechanisms (*vide infra*).

X-Ray Crystallography

The results from the single crystal X-ray diffraction studies of the *tert*-octyl compounds **1e**, **2e**, and **(0e)**_∞ are reported herein. Additionally, we report the crystal structure of the starting material, (OctN)₂MoCl₂·dme, in the supporting information. A summary of selected bond lengths and angles is provided in Table 1 and additional crystallographic parameters and images can be found in the supporting information. In both the tmeda adduct **1e** and the bpy adduct **2e**, the molybdenum centers have octahedral coordination environments with the chlorides orientated *trans* to each other in both structures. The Mo–N(tmeda) bond lengths in **1e** are similar to the corresponding lengths in other tmeda adducts [2.525(7) and 2.556(7) Å (**1a**);²⁸ 2.512(4) and 2.529(3) Å (**1b**);³⁶ 2.508(6) and 2.532(7) Å (**1c**);³⁶ 2.499(2) and 2.554(2) Å (**1d**)³⁶], suggesting that the binding of tmeda is not affected by the alkyl chain length of the imido groups; a similar result is observed for **2e** when compared to the bpy adducts **2a-c**. In both **1e** and **2e** the Mo–N(imido) bond lengths are consistent with those in other (RMe₂N)₂MoCl₂·L (L = *N,N'*-chelating ligand) compounds. The average imido bond angles in both **1e** and **2e** are similar to the average imido angles of the other compounds we recently reported.³⁶ Although a slight deviation from linearity is observed, this has been shown to be caused by steric repulsion and crystal packing forces,^{53,54} and the energy associated with the imido bending is very low.^{55,56} The *tert*-octylimido ligands also provide the

largest buried volume⁵⁷ ($\%V_{\text{bur}} = 40.2$, Figure S49) of all the *tert*-alkylimido adducts studied, as the long alkyl chains can wrap around the molybdenum atom. Finally, *tert*-octyl imido ligands are relatively rare and under explored, as highlighted by a search of the Cambridge Structural Database⁵⁸ which revealed only two other structures containing *tert*-octyl imido ligands, $[(^t\text{OctN})\text{OsO}_3]_2 \cdot \text{N}_2\text{C}_6\text{H}_{12}$ ⁵⁹ and $(^t\text{OctN})\text{TaCl}_3 \cdot \text{dme}$.⁶⁰

Table 1. Selected bond lengths and angles of the $(^t\text{OctN})_2\text{MoCl}_2$ adducts.

Compound	Mo–N(chelate) / Å	Mo–N(imido) / Å	Mo–N–C deg	Cl–Mo–Cl/ deg
1e	2.5121(9)	1.7407(9)	161.92(8)	161.776(10)
	2.5637(10)	1.7498(9)	163.22(9)	
2e	2.3889(7)	1.7526(8)	156.56(7)	159.380(8)
	2.3498(7)	1.7431(8)	164.19(18) ^a	
(0e)_∞	--	1.7282(15)	169.60(12)	158.785(14)
		1.7438(15)	151.02(12)	77.179(14) ^b

[a] Bond angle for Part A; Part B Mo1–N4–C19b = 164.4(3)°. [b] Angle between the bridging chlorides of the dimeric unit, Cl1–Mo1–Cl1[#]; # symmetry transformation: 1–x, 1–y, –z.

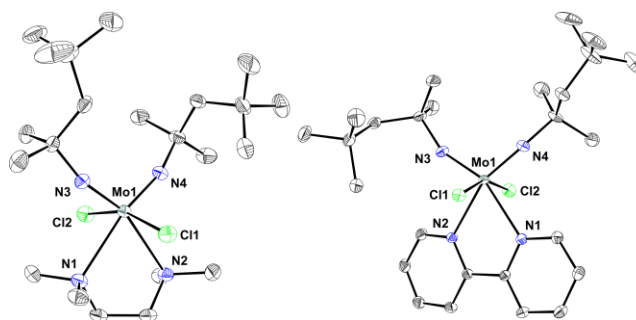


Figure 1. Solid-state structures of $(^t\text{OctN})_2\text{MoCl}_2 \cdot \text{tmeda}$ (**1e**, left) and $(^t\text{OctN})_2\text{MoCl}_2 \cdot \text{bpy}$ (**2e**, right). Thermal ellipsoids are drawn at the 50% probability level. Hydrogen atoms have been omitted for visual clarity. The $\text{C}(\text{CH}_3)_3$ moiety of the *tert*-octyl group (on N3) in **1e** and the entire *tert*-octyl group (on N4) in **2e** are disordered over two positions, however, only Part A of the disorder is shown for visual clarity.

Unlike the dimer of $(^t\text{BuN})_2\text{MoCl}_2$ which has bridging imido ligands, $[(^t\text{BuN})\text{Mo}(\mu\text{-N}^t\text{Bu})\text{Cl}_2]_2$ (**0a**)₂,²⁸ the *tert*-octyl analogue (**0e**)_∞ dimerizes through bridging chloride ligands (Figure 2). However, the dimeric units in (**0e**)_∞ are not discrete, instead forming extended polymeric chains through the formation of additional chloride bridges between Mo centers. This results in chains of edge-sharing octahedral centers ($[(^t\text{OctN})_2\text{Mo}(\mu\text{-Cl})_2]_\infty$, Figure 2), similar to those observed in the polymeric structure of ZrCl_4 .⁶¹ This additional chloride bridge makes the molybdenum in (**0e**)_∞ hexacoordinate, whereas the molybdenum centers in the discrete dimeric units of the *tert*-butyl analogue (**0a**)₂ are pentacoordinate, with a distorted geometry that falls between trigonal bipyramidal and square pyramidal ($\tau_5 = 0.49$).²⁸

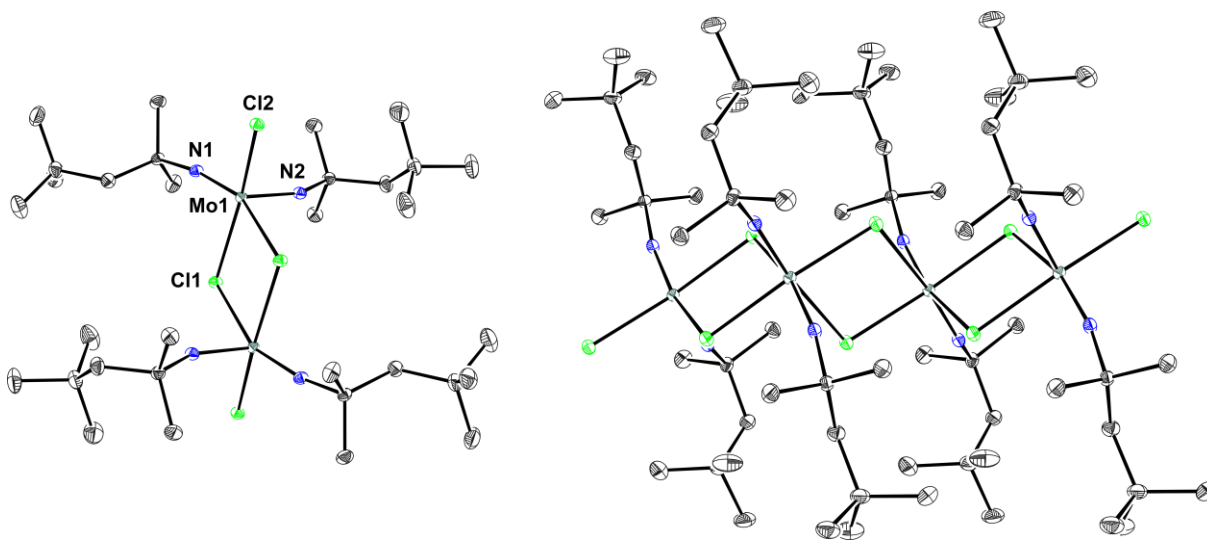


Figure 2. Solid-state structure of $[(^t\text{OctN})_2\text{Mo}(\mu\text{-Cl})_2]_\infty$ (**0e**)_∞ showing the dimeric unit (left) and the extended polymeric structure (right). Thermal ellipsoids are drawn at the 50% probability level. Hydrogen atoms have been omitted for visual clarity.

The Mo–N bond of one of the imido ligands in **(0e)**_∞ is significantly shorter than the other, as well as being shorter than the imido bonds in the other *tert*-octyl imido adducts **1e** and **2e** (Table 1). This is likely due to additional electron contribution from its nitrogen (N1) because **(0e)**_∞ is coordinatively saturated with bridging chloride ligands, which are less Lewis basic than the *N,N'*-chelates. The chloride bridges in the dimeric unit of **(0e)**_∞ are unsymmetrical [Mo1–Cl1 = 2.4561(4) Å, Mo1–Cl1(1–*x*, 1–*y*, –*z*) = 2.6482(4) Å], similar to those in the *tert*-butylamine adduct, [(^tBuN)₂MoCl(μ-Cl)·(^tBuNH₂)₂]₂.⁷ The extended polymeric structure **(0e)**_∞ has further unequal bridging chloride interactions [Mo1–Cl2 = 2.4071(4) Å and Cl2(1–*x*, –*y*, –*z*)...Mo1 = 2.9086(4) Å]. The imido ligand *trans* to this longer interaction has the longer Mo–N bond length in **(0e)**_∞, whereas the shorter imido bond is *trans* to the Mo1–Cl1(1–*x*, 1–*y*, –*z*) bond. This likely forms a stronger interaction due to the *trans*-effect imposed by the shorter imido ligand. Finally, the polymeric chains run parallel to the *Y*-axis, with only a few weak CH...H intermolecular interactions between each chain.

In Situ Thermolysis Reactions

We performed a series of thermolysis studies to identify the decomposition products of the bis(alkylimido)-dichloromolybdenum(VI) compounds to help elucidate their thermal reaction mechanisms. We began with solution phase thermolysis reactions; the compounds were heated in C₆D₆ in sealed NMR tubes under vacuum, and the reactions were monitored periodically by *ex situ* ¹H NMR spectroscopy. First, we investigated the solution phase thermolysis of the tmeda adduct **1a** by closely monitoring its reaction progress (Figure 3). We chose this compound as a primary model for the (^tBuN)₂MoCl₂ adducts because the tmeda ligand provided an excellent spectroscopic handle and **1a** had one of the lowest *T*_D by DSC.³⁶

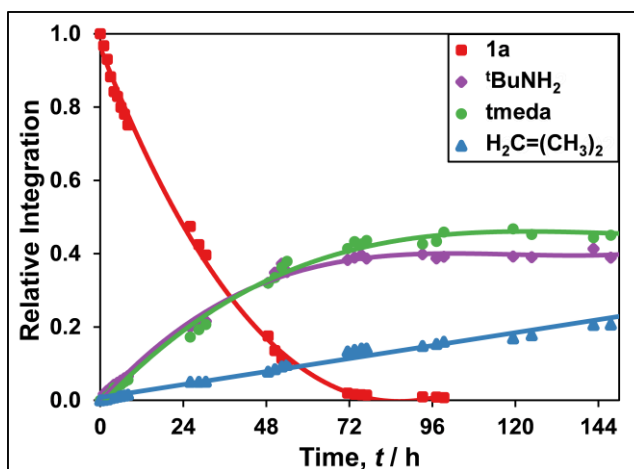
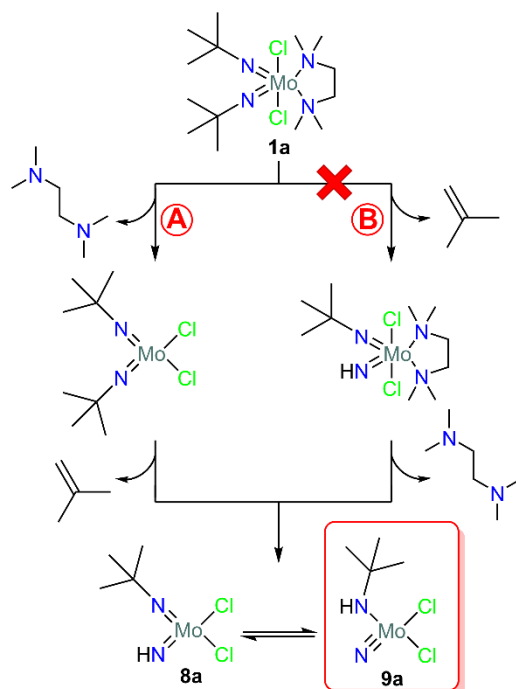


Figure 3. Rate of decomposition of $(t\text{BuN})_2\text{MoCl}_2 \cdot \text{tmeda}$ (**1a**, red square), and related rates of formation of *tert*-butylamine (purple diamond), tmeda (green circle) and isobutylene (blue triangle) in C_6D_6 at 185 °C. The ^1H NMR spectra are shown in Figure S9.

After holding the C_6D_6 solution of **1a** at 175 °C overnight, ^1H NMR spectroscopy did not reveal any decomposition, despite being above the T_D determined by DSC. The mixture was then heated to 185 °C and decomposition was observed almost immediately. The relative concentration of **1a** decreased until it had been entirely consumed after 96 h. Compound **1a** decomposed following first order kinetics with a half-life of 24 h. Additionally, signals for free tmeda (^1H NMR (C_6D_6) $\delta = 2.35$ and 2.12 ppm, Figure S10) were observed to increase as did signals arising from the formation of isobutylene (^1H NMR (C_6D_6) $\delta = 4.75$ and 1.59 ppm, Figure S10). Isobutylene likely results from the γ -H activation of the *tert*-butyl group.^{7,8,28–30,36} Finally, alongside the formation of isobutylene and tmeda, a singlet at 1.00 ppm, which has been ascribed to *tert*-butylamine (^1H NMR (C_6D_6) $\delta = 0.99$ and 0.67 ppm, Figure S10), was also found to increase in intensity. However, the NH_2 protons of *tert*-butylamine were not detected. Throughout the course of the thermolysis, a dark colored, metallic appearing film was slowly deposited on the inside of the NMR tube. We

never observed a mono-imido intermediate, possibly because this is not a stable intermediate, or perhaps it is insoluble in C₆D₆. It should also be noted that the relative ratios of products could not be reliably quantified using this method because some of the byproducts are gaseous under standard conditions and are likely partitioned between the solution and the headspace of the sealed NMR tube.

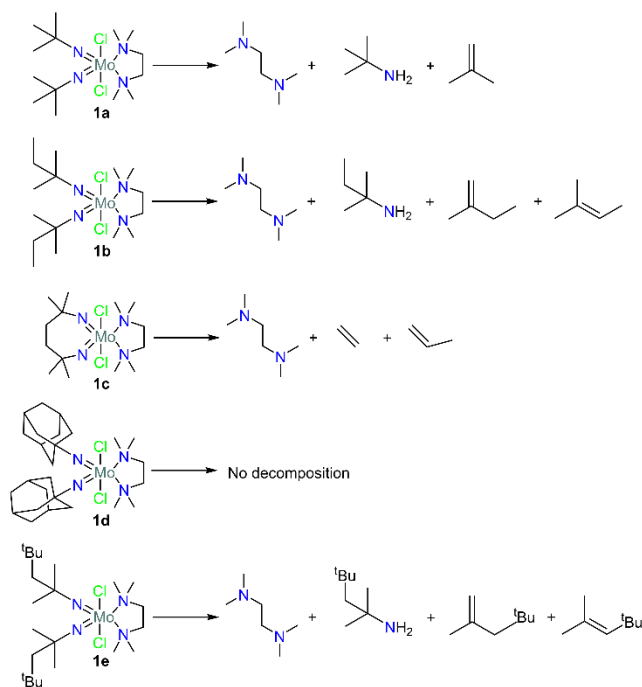
The observation of both free tmeda and isobutylene suggests that there are two major decomposition pathways available to **1a** (Scheme 2). In pathway A, tmeda first dissociates from **1a** resulting in the formation of (tBuN)₂MoCl₂, and then the unligated (tBuN)₂MoCl₂ **0a** or its dimer [(tBuN)Mo(μ-N^tBu)Cl₂]₂ (**0a**)₂ undergoes γ-H activation to eliminate isobutylene (*T*_D = 175 °C).²⁸ In pathway B, **1a** does the opposite, it first undergoes γ-H activation to eliminate isobutylene, followed by tmeda dissociation from the resulting species. It has been proposed that compounds of the general structure (tBuN)₂MX₂ (M = Mo or W, X = anionic ligand) eliminate isobutylene *via* γ-H activation and form a hydrogen-substituted imido complex (**8a**).^{8,9,30,62–64} However, H-substituted imido ligands are relatively acidic (p*K*_a ~10-15),^{30,65} and it is likely that they would be deprotonated, resulting in further decomposition. Instead, we propose that the product of thermolysis is a nitrido-amido complex (**9a**). Furthermore, if the hydrogen-substituted imido was the initial product of thermolysis, it would likely undergo an intra- or intermolecular H-transfer to give **9a** since the alkyl imido moiety is quite basic (p*K*_a ~ 16-20).^{66,67} The observation of *tert*-butylamine also supports our proposal because formation of the protonated amide must be the first step in generating the primary amine. Finally, compound **9a** contains a triple-bonded Mo≡N moiety, which has been observed in films prepared using (tBuN)₂MoX₂ (X = anionic ligand) compounds as single-source precursors in CVD.^{7,8,10,29,30}



Scheme 2. Two proposed pathways for the thermal decomposition of $(^t\text{BuN})_2\text{MoCl}_2 \cdot \text{tmeda}$ (**1a**). Only the first two steps of the thermolysis are shown; refer to Scheme 4 for the full decomposition.

To determine the generality of this proposed decomposition pathway we also performed solution-phase thermolysis of some of our other adducts. For example, the bpy adduct **2a** was determined to be quite thermally stable; the decomposition at 185 °C followed first-order kinetics with a calculated half-life of 107 h, suggesting that appreciable decomposition would not happen under most precursor delivery conditions. Despite the thermolysis of **2a** occurring significantly below its T_D measured by DSC (272 °C),³⁶ the observed decomposition was likely due to the lability of the bpy ligand (*vide infra*). Indeed, signals for free bpy were observed alongside those attributed to isobutylene and *tert*-butylamine throughout the thermolysis. Again, isobutylene, *tert*-butylamine, and free ^tBu dad were also observed during the thermolysis of the diazabutadiene adduct **3** which was carried out at 185 °C over 2 days.

To probe the thermal decomposition mechanism more carefully, we subjected several *tert*-alkylimido analogues of **1a** to the same type of solution-phase thermolysis study (Scheme 3). Thermolysis of the *tert*-pentyl tmeda adduct **1b** and the *tert*-octyl tmeda adduct **1e** were similar to that of the *tert*-butyl analogue **1a**. Heating **1b** to 175 °C for 24 h resulted in the formation of free tmeda, but no γ -H activation products, suggesting a stepwise thermolysis potentially starting with dimer formation. Upon heating the solution to 185 °C for 24 h, signals for *tert*-pentylamine and both the Zaitsev and Hofmann elimination products, 2-methyl-2-butylene and 2-methyl-1-butylene, respectively, were observed. *In situ* thermolysis of the *tert*-octyl adduct **1e** gave results similar to those of **1a** and **1b**. After heating **1e** to 185 °C for 24 h, we observed free tmeda, *tert*-octylamine, and two alkenes: 2,4,4-trimethyl-1-pentene (Hofmann product) and 2,4,4-trimethyl-2-pentene (Zaitsev product), with the latter being quite minor (*ca.* 16%) relative to the former. These results are also supported by solid-state thermolysis experiments (*vide infra*).



Scheme 3. Summary of the decomposition products observed using ^1H NMR spectroscopy for the *in situ* thermolysis of the tmeda adducts **1a-e**. All thermolysis reactions were performed in C_6D_6

at 185 °C in flame-sealed NMR tubes. Molybdenum-containing intermediates were not observed in any reaction. The relative ratio of products is not shown. Solid black particles (e.g., $\text{MoC}_x\text{N}_y\text{Cl}_z$) were observed in most samples.

In situ thermolysis of the tethered imido tmeda adduct **1c** at 185 °C initially resulted in the formation of a black precipitate, and the ^1H NMR spectrum revealed only signals arising from tmeda. Further heating of the sample gave signals that have been tentatively assigned to ethylene and propylene. Ethylene would result from the homolytic cleavage of the C_2H_4 moiety on the backbone of the ligand. We propose that a bis(ketimide)dichloromolybdenum(IV) compound is being formed, which is supported by the EI-HRMS results (*vide infra*). This putative Mo(IV) species subsequently undergoes further decomposition to $\text{MoC}_x\text{N}_y\text{Cl}_z$ (observed as a black particulate) and propene. Similar C_2H_4 liberation has also been observed for 2,5-dimethylhexane-2,5-diamine.⁶⁸ Finally, *in situ* thermolysis of the adamantyl tmeda adduct **1d** did not show any decomposition after 72 hours at 185 °C, likely due to Bredt's rule:⁶⁹ the bridgehead alkene that would exist in the eliminated adamantene,⁷⁰ the proposed γ -H activation product of **1d**, are rare and often unstable. At these temperatures the chelating tmeda is likely labile, however, because the thermolysis was performed in a closed system, the adduct was easily reformed when the NMR tube was removed from the oven and cooled sufficiently to handle, and so free tmeda was not observed.

Solid-State Thermolysis Reactions

To further elucidate the mechanism proposed in Scheme 2, we chose to re-investigate the thermal properties of the adamantyl tmeda adduct **1d**. We had previously found that **1d** has low volatility

but high thermal stability, unlike the other *tert*-alkyl substituted tmeda adducts.³⁶ This suggested it might be a good candidate from which to examine our proposed decomposition pathway in the solid state using thermogravimetric analysis (TGA). Using **1d** allowed us to deconvolute the mass loss due to ligand dissociation from the mass loss due to vaporization of the adduct, whereas the other adducts **1a-c** and **1e** experience both vaporization and decomposition around 170 °C. Ramped TGA of **1d** revealed a thermal event beginning at 170 °C which resulted in a 20% mass loss and then further mass-loss events occurring at higher temperatures (Figure 4a). Isothermal analysis of **1d** at 170 °C showed the product with 80% residual mass to be stable and non-volatile, which corresponds to it having lost the tmeda ligand (Figure 4b). These results support our proposed decomposition mechanism: upon heating **1d** tmeda dissociates and evaporates first, presumably leaving behind the unligated (AdN)₂MoCl₂, which then undergoes further decomposition at higher temperatures.

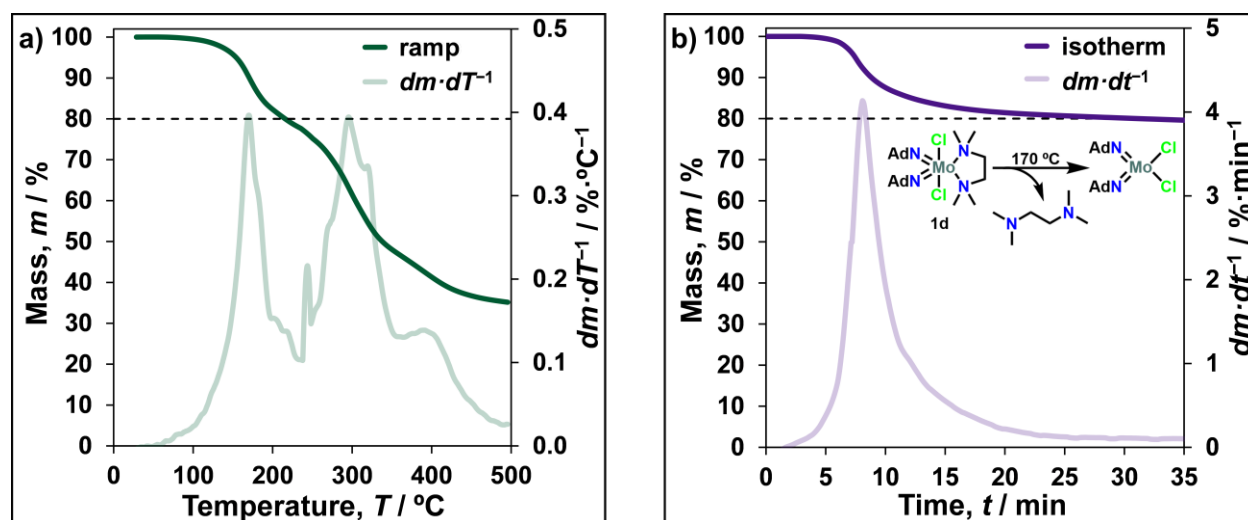


Figure 4. (a) Thermogravimetric analysis of (AdN)₂MoCl₂·tmeda (**1d**), with a heating rate of 5 °C min⁻¹ and (b) isothermal analysis of **1d** at 170 °C. For the isothermal analysis the sample was heated at 20 °C min⁻¹ and then was held at 170 °C. The mass loadings were 10.0 ± 0.1 mg for each

sample. A horizontal line is shown at 80% residual mass, which corresponds to the mass loss of tmeda (as shown in the inset).

Preparative-scale solid-state thermolysis studies were used to analyze the decomposition products. The *tert*-butyl tmeda adduct **1a** was heated to *ca.* 200 °C in a sealed flask under static vacuum (40 mTorr) for 30 minutes. After complete decomposition, the volatile byproducts were trapped in a receiving flask cooled to -75 °C, leaving behind a shiny black residue in the reaction vessel. Note that it was necessary to collect the volatile decomposition byproducts only after complete thermolysis because **1a** itself is volatile and sublimates under dynamic vacuum. The only volatile products collected were tmeda, *tert*-butylamine, and isobutylene, as determined using ^1H NMR spectroscopy. Significantly less isobutylene was collected than was expected for complete decomposition, but it was likely lost during workup of the byproducts due to its high volatility (b.p. = -7 °C).⁷¹

The shiny black non-volatile residue from the solid-state thermolysis of **1a** was analyzed using transmission electron microscopy (TEM), energy-dispersive X-ray spectroscopy (EDS) and electron diffraction. It was determined to be an amorphous solid with the empirical formula $\text{MoC}_x\text{N}_y\text{Cl}_z$ and a Mo:Cl ratio of approximately 1:1 (Figure S18). After the sample was annealed at 350 °C, the solid crystallized into tetragonal β - Mo_2N (Figure 5), which was identified by the d-spacings of 2.29 Å and 2.40 Å, which correspond to the (103) and (112) faces of β - Mo_2N respectively.^{37,72} These results suggest $(^t\text{BuN})_2\text{MoCl}_2\cdot\text{L}$ (L = neutral *N,N'*-chelate) compounds could find application as single-source precursors for the CVD of crystalline β - Mo_2N .

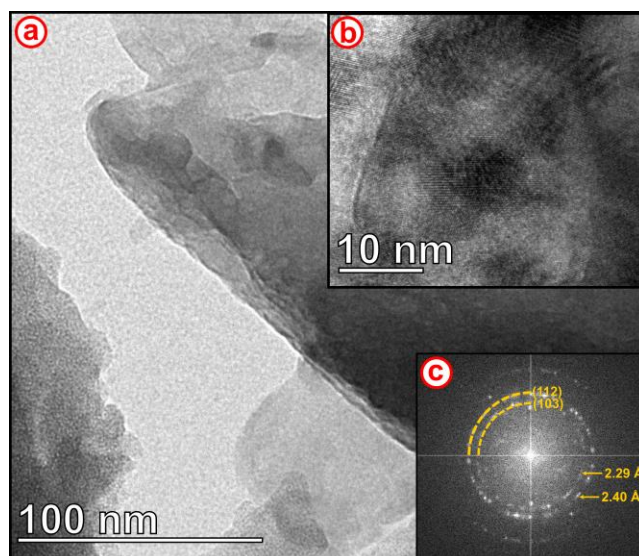


Figure 5. (a) TEM of the residue obtained from the solid-state thermolysis of $(t\text{-BuN})_2\text{MoCl}_2 \cdot \text{tmeda}$ (**1a**), after annealing at 350 °C. (b) High-resolution TEM of the particles and (c) its fast Fourier transform showing the (103) ($d = 2.29 \text{ \AA}$) and (112) ($d = 2.40 \text{ \AA}$) fringes of tetragonal $\beta\text{-Mo}_2\text{N}$.

To obtain more quantitative results from the analysis of the decomposition byproducts we moved to the *tert*-octyl analogue **1e** since its expected γ -H activation product 2,4,4-trimethyl-1-pentene is a liquid under standard conditions (b.p. = 101 °C),⁷¹ which would greatly simplify collection for characterization and quantification. After heating the *tert*-octyl tmeda adduct **1e** to *ca.* 200 °C for 30 minutes, the volatile byproducts were collected and characterized using ^1H NMR spectroscopy and gas chromatography - mass spectrometry (GC-MS, Table 2). Both the internal (Zaitsev) and external (Hofmann) alkene products were again observed, with the latter being more abundant despite internal alkenes being favored thermodynamically. This is likely a statistical result (e.g., there are more protons available to undergo the γ -H activation that results in the external alkene). The combined results from *ex situ* ^1H NMR spectroscopy and GC-MS analysis showed that

thermolysis of the *tert*-octyl tmeda adduct **1e** results in two equivalents of the mixture of alkenes being generated per equivalent of *tert*-octylamine.

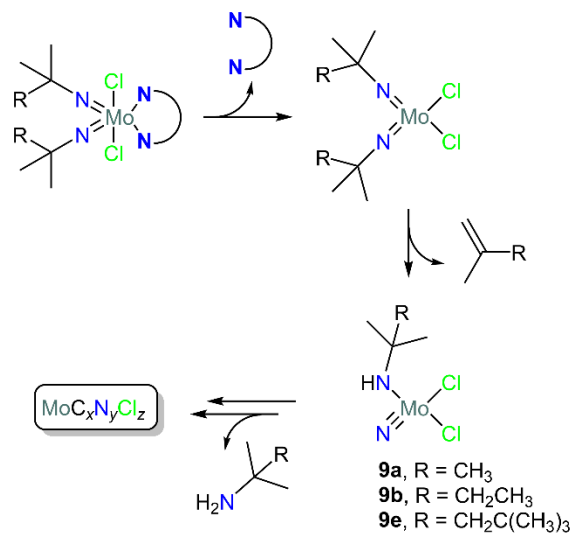
Table 2. Composition of the volatile byproducts from the solid-state thermolysis of $({}^t\text{OctN})_2\text{MoCl}_2\cdot\text{tmeda}$ (**1e**). ${}^1\text{H}$ NMR was performed in C_6D_6 and GC-MS was performed in methanol.

Component	Relative Amount ^a	
	${}^1\text{H}$ NMR	GC-MS
2,4,4-trimethyl-1-pentene	1.00	1.00
2,4,4-trimethyl-2-pentene	0.30	0.49
<i>N,N,N',N'</i> -tetramethyl-ethylenediamine	0.65	0.60
<i>tert</i> -octylamine	0.66	0.74

[a] Relative to the most abundant component, 2,4,4-trimethyl-1-pentene.

The detection of free alkylamines in the *ex situ* solid-state and the *in situ* solution-phase thermolysis experiments led us to postulate an alternative mechanism for the decomposition of the bis(alkylimido)molybdenum(VI) compounds (Scheme 4). We believe that the neutral *N,N'*-chelate first dissociates from the metal center, resulting in the formation of the unligated monomer $(\text{RMe}_2\text{N})_2\text{MoCl}_2$ (or its dimer, bridging through either an imido, (**0a**)₂, or a chloride, (**0e**)_∞). Next one of the imido nitrogen atoms abstracts a γ -H from the other imido moiety. In fact, the solid-state structure of $[({}^t\text{BuN})\text{Mo}(\mu\text{-N}{}^t\text{Bu})\text{Cl}_2]_2$ (**0a**)₂ contains a short $\gamma\text{-H}\dots\text{N}$ intramolecular interaction (2.60 Å)²⁸ and it has previously been shown that the analogous imido group in similar compounds is fairly basic.^{66,67,73,74} This would result in the liberation of an alkene, and the formation of the nitrido-amido moiety **9** (Scheme 4); a similar step has previously been proposed by McElwee-White *et al.* during the thermal decomposition of $({}^t\text{BuN})_2\text{Mo}(\text{S}{}^t\text{Bu})_2$.²⁹ Further thermolysis of the nitrido-amido compound **9** then liberates the free alkylamine, likely through the

combination of two equivalents of **9**, also resulting in the formation of $\text{MoC}_x\text{N}_y\text{Cl}_z$. Although the analysis of the residue revealed a Mo:Cl ratio of 1:1, it is uncertain how the excess chlorine leaves. It has been suggested that volatile MoCl_5 is formed,⁷ and the thin films prepared from single-source CVD of similar compounds have also shown negligible, or non-detectable, chlorine contaminants.^{7,75–79}



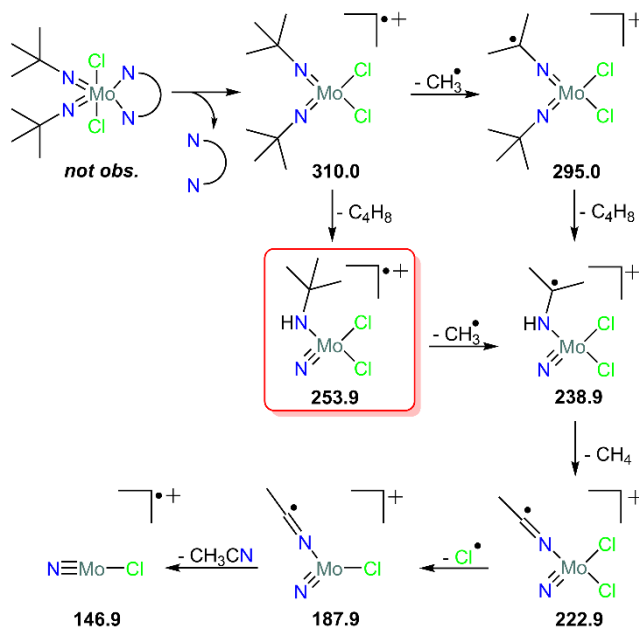
Scheme 4. Proposed thermal decomposition pathway of the $(\text{RMe}_2\text{N})_2\text{MoCl}_2 \cdot \text{L}$ (L = neutral N,N' -chelate) compounds. Only the terminal alkene is shown, however, in some instances the internal alkene also forms (**1b** and **1e**).

Finally, in our previous study involving standard thermal characterization of the xy^l dad adduct **4**, we observed an “ancillary ligand-centered decomposition”.³⁶ This appears to be due to the formation of $(xy/N)_2\text{MoCl}_2 \cdot {}^t\text{Bu}^l\text{dad}$, through an intramolecular imine metathesis with the diazabutadiene fragment $(\text{RN}=\text{CHR}')$;^{80–82} a similar reaction has been observed for the titanium imido adduct, $({}^t\text{BuN})\text{TiCl}_2 \cdot 3\text{py}$. Detailed discussion of this decomposition is beyond the scope of this study and therefore it has been placed in the supporting information.

Mass Spectroscopy Fragmentation Analysis

It is well established that the fragmentation patterns of precursors, obtained from mass spectrometry, can be correlated to plausible decomposition pathways during CVD.^{78,79,83–85} For example, ionization can reveal the weakest bonds, which often correspond to the first bonds to break under thermally induced decomposition. Electron ionization high-resolution mass spectrometry (EI-HRMS) was used to gain further insight into the stability and potential decomposition pathways of several of our compounds. EI-HRMS of the (^tBuN)₂MoCl₂ adducts containing the three main classes of ligands (tmEDA, **1a**; bpy, **2a**; ^tBu₃dad, **3**) all gave identical results (Scheme 5). Most notably, the M⁺ ion was not detected in any sample, likely because the source temperature (250 °C) was greater than the decomposition temperatures of these compounds. The fragment with the highest observed mass for each compound had an *m/z* of 309.9, which corresponds to [(^tBuN)₂MoCl₂]⁺ (M⁺ after loss of the *N,N'*-chelating ligand). In all of the samples, the most abundant ion was detected at 238.9 *m/z*, which corresponds to the nitrido-amido **9a** (after the loss of a CH₃ radical) which we also speculate to be the major thermolysis product (Scheme 5). Further fragmentation gives ions with *m/z* of 222.9 and 187.9 which result from β-methyl activation of the *tert*-butyl imido ligands. This accounts for the detection of MeCN when (^tBuN)₂Mo(HN^tBu)₂ (**B**) and (^tBuN)₂MoCl₂·2py (**E**) were used as a single-source CVD precursors.^{7,8} Additionally, none of the abundant fragments correspond to the loss of a chloride ion, further suggesting that these compounds do not decompose through the fragmentation of an Mo–Cl bond (such as by the loss of HCl). Furthermore, most of the fragments observed contained "Mo≡N" moieties, revealing the stability of the molybdenum imido bonds. In fact, Bertuch *et al.* found that only O₃ above 250 °C, was able to crack the Mo=N bond in (^tBuN)₂Mo(NMe₂)₂, whereas

at lower temperatures incomplete ligand removal was observed.¹¹ This further highlights the suitability of $(t\text{BuN})_2\text{MoCl}_2\cdot\text{L}$ compounds for the single-source CVD of MoN_x .



Scheme 5. Most abundant ($\geq 3\%$) molybdenum-containing fragments observed in the EI-HRMS of $(t\text{BuN})_2\text{MoCl}_2\cdot\text{tmeda}$ **1a**. Identical fragments were observed for all of the $(t\text{BuN})_2\text{MoCl}_2$ adducts. The mass spectra can be found in the SI and identification of all fragments is supported by accurate masses and isotopic distributions. The ionized N,N' -chelating ligands were also detected in all cases. The key nitrido-amido intermediate **9a** is outlined in red.

The mass spectrometry results of the other tmeda adducts followed the same general reaction path as seen for **1a** and are consistent with observations from the *in situ* thermolysis reactions. For example, the most abundant ion observed for the *tert*-pentyl and *tert*-octyl tmeda adducts (**1b** and **1e**) had an m/z of 238.9, which corresponds to the mass of the 2-propynyl radical fragment of the nitrido-amido **9** minus the mass of the largest alkyl moiety attached to the tertiary carbon (**9b** – $\bullet\text{C}_2\text{H}_5$ for **1b**, and **9e** – $\bullet\text{C}_5\text{H}_{11}$ for **1e**). Thus, **1b** and **1e** likely undergo the same decomposition

pathway as **1a**, which further supports the general structure **9** being the main thermolysis product. Mass spectrometry of the adamantyl tmeda adduct of **1d** did not exhibit any notable fragmentation products, further showcasing the stability of the adamantyl moiety. Again, M^+ was not detected but $[(AdN)_2MoCl_2]^+$ (i.e., after tmeda loss) was the most abundant ion. Finally, EI-HRMS of the tethered imido adduct **1c** showed fragmentation of the tethered ring and elimination of C_2H_4 . This results in the formation of the putative acyclic bis(ketimide)dichloromolybdenum(IV) (see the SI for additional fragmentation), consistent with the thermal decomposition seen in the *in situ* thermolysis. The thermal instability of M(IV) ketimide adducts has previously been explored by Hayton *et al.*^{86,87}

Computational Investigation

The experimental results showed that bis(alkylimido)-dichloromolybdenum(VI) adducts decompose to form alkenes and free alkylamines, but whether they decompose *via* Pathway A or B (Scheme 2) could not be discerned. Also, it was unclear why some neutral ligands (bpy, phen) showed significant improvements in the thermal stability of the resulting Mo(VI) complexes while others (dad, tmeda) did not. To better understand the decomposition processes of this class of precursors, we used computational chemistry to investigate the decomposition mechanisms of the adducts, the free dimer, $[(^tBuN)Mo(\mu-N^tBu)Cl_2]_2$ (**0a**), and the monomer, $(^tBuN)_2MoCl_2$ **0a**. We focused our computational efforts on finding the lowest energy decomposition reaction of the parent complexes only. While the decomposition reactions that occur after the first event are important for CVD and ALD process mechanisms themselves, they play only a minor role in the thermal stability of the precursor during evaporation and are outside the scope of this study. Recently, very efficient and highly accurate methods have become available in ORCA 5⁸⁸ that

enabled us to investigate many reasonable decomposition mechanisms without needing to resort to reduced model systems or unreliable theoretical methods. We used the efficient implementation of the composite density functional theory (DFT) method r^2 SCAN-3c⁸⁹ to obtain accurate geometries with a low computational cost, and the climbing image nudged-elastic band (NEB-CI)⁹⁰ method to quickly find minimum energy paths (MEPs) and good guess geometries of transition states (TSs) for complicated mechanisms. All proposed reaction mechanisms were confirmed by intrinsic reaction coordinate (IRC) analysis. Finally, highly reliable electronic energies were obtained for all geometries with the domain-based pair natural orbital coupled-cluster theory with singles, doubles, and perturbative triples [DLPNO-CCSD(T)]^{91,92} method to avoid the pitfalls typically associated with using DFT for transition metal complexes and transition state energies. All reported energies for minima and saddle points were obtained with the DLPNO-CCSD(T)/def2-TZVPP// r^2 SCAN-3c method in the gas phase unless otherwise noted.

Initially, it was hypothesized that every neutral ligand stabilized the Mo(VI) adducts and that the differences in their decomposition temperatures were due to the relative bond strengths of the neutral ligand to the metal ion. If this was true, decomposition would primarily occur *via* the free dimer (or monomer) only after the neutral ligand had dissociated. In an earlier study,²⁸ we found that weakly bound ligands (i.e., 1,2-dimethoxyethane (dme), BDE = 21.2 kcal·mol⁻¹) would dissociate completely upon heating to form the free dimer [(^tBuN)Mo(μ -N^tBu)Cl₂]₂ (**0a**)₂. While the incorporation of dme improved the volatility of the adduct, it did not improve the overall thermal stability of the free unligated dimer (**0a**)₂ that began to decompose at 170 °C.²⁸ In our preceding study,³⁶ we found that some ligands, like 1,10-phenanthroline, dramatically improved T_D (by more than 100 °C), albeit at the expense of volatility. We also found that a compromise could be achieved by combining one symmetric ligand with high thermal stability (e.g., bpy, **2a**)

with another symmetric ligand having high volatility (e.g., ^tBu₂dad, **3**) in an unsymmetric hybrid ligand (e.g., impy, **6**) containing both coordinating moieties. Unfortunately, correlations were not found between the computed bond dissociation enthalpy (BDE, ΔH) or the bond dissociation free energy (BDFE, ΔG) of each neutral ligand from its respective Mo(VI) adduct with the decomposition temperatures observed by DSC (Table 3, $R^2 = 0.276$ and 0.416 , respectively). So, we set out to investigate the nuances of other decomposition mechanisms more carefully.

Table 3. Computed^[a] free energy and enthalpy changes (in kcal·mol⁻¹) of ligand dissociation and forward barrier energies of γ -H elimination reactions for free (^tBuN)₂MoCl₂ and its adducts with various ligands.

Compound	Ligand	$T_D / ^\circ\text{C}^{36}$	BDFE ^[b] ΔG	BDE ^[b] ΔH	ΔG^\ddagger ^[c] Mo=NH	ΔG^\ddagger ^[d] Mo≡N
0a	—	175	—	—	63.8	40.1
(0a) ₂	0a	175	7.9	24.5	55.2 ^[c]	37.3
1a	κ_2 -tmeda	174	18.5	34.1	68.2	42.8
2a	κ_2 -bpy	272	18.8	33.1	72.3	43.1
3	κ_2 -dad	170	8.0	24.5	65.2	44.7
5	κ_2 -phen	303	19.9	34.5	69.2	42.4
6	κ_2 -impy	232	17.5	33.3	68.0 ^[f] 67.7 ^[g]	44.7 ^[f] 42.8 ^[g]
7	κ_2 -dmampy	200	16.7	31.6	69.0 ^[f] 67.4 ^[h]	40.8 ^[f] 41.7 ^[h]

[a] Computed with DLPNO-CCSD(T)/def2-TZVPP//r²SCAN-3c under standard conditions (1 bar and 25 °C). [b] Using the lowest energy conformers of dissociated neutral free ligand and free monomer **0a** at infinite separation. [c] Decomposition to the hydrogen-terminated imido. [d] Decomposition to the nitrido-amido. [e] DLPNO-CCSD(T)/def2-TZVPP//revPBE-D3(BJ)/def2-SVP(Mo=def2-TZVPP) level of theory; analogous saddle point could not be found with r²SCAN-3c. [f] ^tBuN group *trans* to the pyridyl of impy or dmampy. [g] ^tBuN group *trans* to the ^tBuN=CH of impy. [h] ^tBuN group *trans* to the NMe₂ of dmampy.

Previously, we and others have proposed that bis(*tert*-butylimido)-dichloromolybdenum(VI) adducts decompose by a γ -H abstraction from the *tert*-butylimido group by the imido group's nitrogen itself, through a four-membered cyclic transition state, to give a hydrogen-terminated imido ligand bound to Mo(VI) (Figure 6a).^{7,28,36} Here, we found that the calculated barriers were far too high ($\Delta G^\ddagger > 65 \text{ kcal}\cdot\text{mol}^{-1}$) for this to be the main decomposition pathway at the temperatures observed in the condensed phase by DSC (*ca.* 170-300 °C). In addition, we found only a weak correlation between the energies of these barriers and the observed decomposition temperatures ($R^2 = 0.553$). On the other hand, the alternative mechanism described above (Scheme 4) involving abstraction of the γ -H by the other *tert*-butylimido group, forming *tert*-butylamido and nitrido moieties bonded to Mo(VI) (i.e., Mo \equiv N), along with free isobutylene, had significantly lower barriers ($\Delta G^\ddagger \sim 40\text{-}45 \text{ kcal}\cdot\text{mol}^{-1}$) for all of the adducts (Table 3). Also, these were higher than the barriers for the unligated bis(*tert*-butylimido)-dichloromolybdenum(VI) monomer **0a** and dimer (**0a**)₂ (40.1 and 37.3 kcal·mol⁻¹, respectively). All of these barriers were higher than the BDEs of the neutral *N,N'*-chelating ligands on the adducts ($\Delta H < 35 \text{ kcal/mol}$). This is consistent with our hypothesis that the ligands dissociate first, then the resulting free bis(*tert*-butylimido)-dichloromolybdenum(VI) monomer or dimer (**0a**)₂ decomposes thereafter. However, the energy barriers of this pathway still did not correlate with the decomposition temperatures observed by DSC (Table 3, $R^2 = 0.004$). Clearly, another pathway must be accessible to some of the adducts, but not others, to explain their different decomposition temperatures.

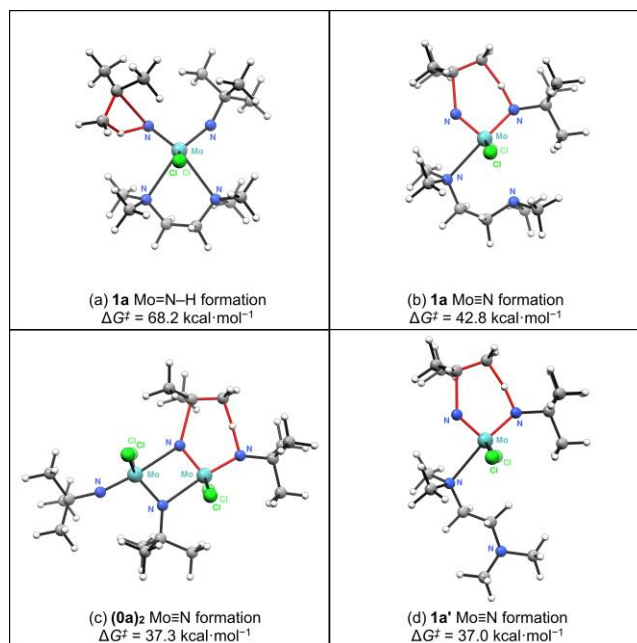
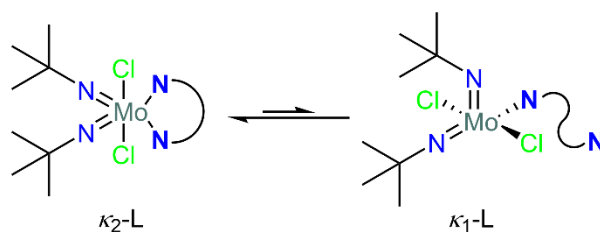


Figure 6. Representative transition states leading toward the formation of isobutylene *via* γ -H elimination in **1a** by (a) formation of a hydrogen-terminated imide (i.e., Mo=N–H) through a four-membered transition state and (b) the formation of *tert*-butylamide and a nitrido moiety (i.e., Mo≡N) through a six-membered transition state. The same transition states are found for the other adduct complexes. (c) Dimeric [(*t*BuN)Mo(μ -N^{*t*}Bu)Cl₂]₂ **3a** and (d) the pentacoordinate isomer **1a'** produced *via* the formation of *tert*-butylamido and nitrido moieties, have the lowest energy barriers found in this study.

Up to this point, only hexacoordinate octahedral isomers of the Mo(VI) complexes, where each neutral chelating ligand had a bidentate configuration (e.g., κ_2 -tmeda in **1a**), had been considered. However, most of the adducts can also conceivably isomerize by an internal rotation of the *N,N'*-chelating ligand to become square pyramidal ($\tau_5^{93} = 0.02$ -0.22) pentacoordinate Mo(VI) complexes with the neutral chelating ligand in a monodentate configuration (e.g., κ_1 -tmeda for **1a**, Scheme 6). Consistent with this hypothesis is our experimental observation that the most thermally stable

complex herein, the 1,10-phenanthroline adduct **6**, was found to have a rigid ligand that could not easily adopt a monodentate configuration ($\Delta G^\ddagger = 42.4 \text{ kcal}\cdot\text{mol}^{-1}$, $T_D = 303 \text{ }^\circ\text{C}^{36}$).



Scheme 6. The isomerization reaction of a $({}^t\text{BuN})_2\text{MoCl}_2\cdot\text{L}$ ($\text{L} = N,N'$ -chelating ligand) complex from the hexacoordinate bidentate $\kappa_2\text{-L}$ configuration (left, more stable) to the pentacoordinate monodentate $\kappa_1\text{-L}$ configuration (right, less stable).

Mechanistically, the pentacoordinate isomers were expected to have lower decomposition barriers than their hexacoordinate analogues by virtue of the reduced steric hindrance of the *tert*-butyl group *cis* to the unchelated side (Figure 6d). Previously, we had found that the pyridine adduct $({}^t\text{BuN})_2\text{MoCl}_2\cdot 2\text{py}$ first loses one pyridine ligand by evaporation, to form $({}^t\text{BuN})_2\text{MoCl}_2\cdot\text{py}$, before decomposing at $183 \text{ }^\circ\text{C}$.²⁸ In the same study, the pentacoordinate *N*-heterocyclic carbene and phosphine adducts also had reduced thermal stabilities compared to the other hexacoordinate complexes studied.²⁸ Preliminary evidence for this was also found in the transition state structures of the hexacoordinate isomers, where the Mo–N bond lengths to the chelating ligands became elongated to make room for the *tert*-butylamido group of the product (e.g., Figure 6b). Fortunately, we found that the pentacoordinate isomers were only slightly higher in energy ($\Delta G_{\text{iso}} < 10 \text{ kcal}\cdot\text{mol}^{-1}$), than the related hexacoordinate isomers, and the minimum energy pathways (MEP) for the isomerization reactions had small barriers ($\Delta G_{\text{MEP}}^\ddagger < 20 \text{ kcal}\cdot\text{mol}^{-1}$) that would be easily overcome at the observed decomposition temperatures (i.e., >170

°C). Also, each pentacoordinate complex had one γ -H that was already proximally close to the nitrogen on the other *tert*-butylimido moiety ($d_{\text{N-H}} \sim 2.8 \text{ \AA}$), so they can be considered reasonable intermediates in the decomposition of the parent complexes. Indeed, the calculated barriers to the decomposition *via* formation of *tert*-butylamido and nitrido moieties (and free isobutylene), were not only significantly lower than those of the hexacoordinate isomers ($37.0 < \Delta G_{\text{penta}}^{\ddagger} < 39.2 \text{ kcal}\cdot\text{mol}^{-1}$), but were also lower than the free monomer and higher than the free dimer for the same pathway (Table 3). Finally, the natural logarithm of the BDFE for the dissociation of the monodentate ligands from the pentacoordinate complexes to yield the dimer (**0a**)₂ showed a strong linear correlation with the decomposition temperature of the parent complexes ($R^2 = 0.917$, Figure 7). Thus, the observed thermal stability of the hexacoordinate complexes was controlled by the free energy of their pentacoordinate isomers relative to their free ligand and dimer (Figure 7).

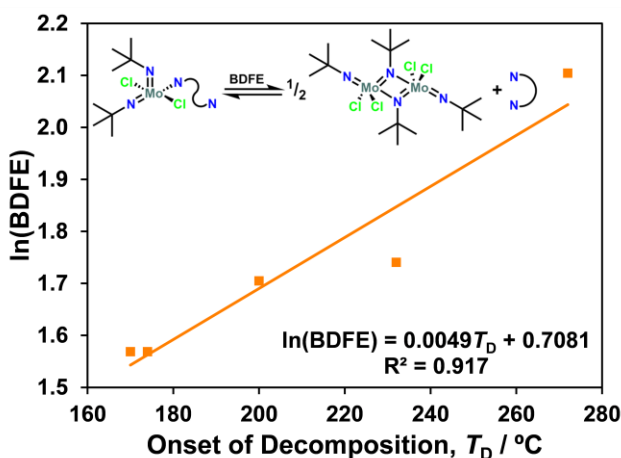


Figure 7. Bond dissociation free energy (BDFE) for the dissociation of flexible ligands from their pentacoordinate bis(*tert*-butylimido)-dichloromolybdenum(VI) complexes to form the free ligand and free dimer (**0a**)₂ (inset) and the correlation of $\ln(\text{BDFE})$ with the onset of decomposition, as observed by DSC, showing that the free energy of the dimer relative to the pentacoordinate

intermediate determines the observed decomposition temperature of the hexacoordinate parent complexes.

The key intermediates controlling the relative decomposition temperatures of the bis(*tert*-butylimido)-dichloromolybdenum(VI) adducts could now be identified using our combined experimental and computational results (Figure 7). First, all ligands had BDEs and BDFEs that were comparable, but lower, than the lowest decomposition barrier enthalpies and energies (i.e., $BDE < \Delta H_{\text{nit}}^\ddagger$ and $BDFE < \Delta G_{\text{nit}}^\ddagger$). This means that there would be significant populations of free monomer, dimer, and ligand present, along with the respective chelated complexes, at elevated temperatures (e.g., >170 °C). The free unchelated dimer, $[(^t\text{BuN})\text{Mo}(\mu\text{-N}^t\text{Bu})\text{Cl}_2]_2$, had the lowest observed thermal stability and also the lowest calculated energy barrier to the γ -H abstraction pathway *via* the endocyclic *tert*-butyl group ($\Delta G_{\text{nit}}^\ddagger = 37.3$ kcal·mol⁻¹, Figure 6c). The highest thermal stability was observed in complex **6** ($T_D = 303$ °C) which contained the strongly bound and rigid 1,10-phenanthroline ligand (BDE = 34.5 kcal·mol⁻¹) and had a relatively high decomposition barrier ($\Delta G_{\text{nit}}^\ddagger = 42.4$ kcal·mol⁻¹). Notably, **6** was the only complex that could not rearrange to form a pentacoordinate intermediate by which to access a lower-energy pathway. The pentacoordinate isomers of the other hexacoordinate adducts had decomposition barriers that were higher than those of the free dimer and lower than those of the free monomer ($37.0 < \Delta G_{\text{penta}}^\ddagger < 39.2$ kcal·mol⁻¹) so their relative contribution to the overall decomposition was determined by the relative population of free dimer. This, in turn, is determined by the BDFE of the monodentate ligand from the pentacoordinate intermediate. Finally, the free energy of the nitrido products of decomposition minus isobutylene had similar free energies to the pentacoordinate adducts, making them reasonable intermediates for subsequent decomposition reactions. Our results suggest that

another generation of hybrid ligands could be designed to combine the rigidity, and thus the thermal stability, conferred by 1,10-phenanthroline with the volatility conferred by some of the other ligands. This precursor design strategy is the subject of an ongoing investigation.

Table 4. Computed^[a] free energy and enthalpy changes (in kcal·mol⁻¹) of ligand dissociation and forward barrier energies of γ -H elimination reactions for free (^tBuN)₂MoCl₂ and the five-coordinate isomers of its adducts with various ligands.

Compound	Ligand	Bound via	$T_D / ^\circ\text{C}^{36}$	ΔG_{iso}	BDFE ^[b] ΔG	BDE ^[b] ΔH	ΔG^\ddagger Mo=N
1a'	κ_1 -tmeda	amine	174	9.6	8.7	23.2	37.0
2a'	κ_1 -bpy	pyridyl	272	6.6	12.1	26.1	38.9
3'	κ_1 -dad	imine	170	-0.8	8.8	23.5	38.5
6'im	κ_1 -impy	imine	232	7.8	9.7	27.7	39.2 ^[d]
6'py		pyridyl		3.9	13.6	27.7	38.4 ^[e]
7'am	κ_1 -dmampy	amine	200	7.2	9.5	24.0	37.4 ^[d]
7'py		pyridyl		6.4	10.3	24.0	38.5 ^[f]

[a] Computed with DLPNO-CCSD(T)/def2-TZVPP//r²SCAN-3c under standard conditions (1 bar and 25 °C). [b] Using the lowest energy conformers of dissociated neutral free ligand and free monomer **0** at infinite separation. [c] DLPNO-CCSD(T)/def2-TZVPP//revPBE-D3(BJ)/def2-SVP(Mo=def2-TZVPP) level of theory; analogous saddle point could not be found with r²SCAN-3c. [d] ^tBuN group *trans* to the pyridyl of impy or dmampy. [e] ^tBuN group *trans* to the ^tBuN=CH of impy. [f] ^tBuN group *trans* to the NMe₂ of dmampy.

Conclusion

The thermal stabilities of a series of bis(alkylimido)-dichloromolybdenum(VI) complexes with various *N,N'*-chelates, have been explored. Upon heating, all compounds initially lose their *N,N'*-chelating ligands as determined using *in situ* ¹H NMR monitoring and thermogravimetric analysis. For the compounds containing *tert*-alkyl (^tBu, ^tPe, ^tOct) imido ligands, the resulting unligated species form a bridging imido dimer, [(RN)Mo(μ -NR)Cl₂]₂. This then undergoes an intramolecular

γ -H transfer to another imido ligand, through a six-membered heterocyclic transition state, as determined using quantum chemical calculations. We also found another low-energy decomposition pathway, that competed with the decomposition of the dimer, which was available to the pentacoordinate isomers of the hexacoordinate parent complexes. The resulting intermediate species contain a *tert*-alkylamido ligand and a nitrido (Mo \equiv N) moiety (**9**) and was detected as the most abundant fragment in the EI-HRMS of all *tert*-alkylimido compounds herein. The formation, isolation, and characterization of primary *tert*-alkylamines, using NMR spectroscopy and GC-MS, provided further evidence for the proposed γ -H transfer. Promisingly, thermolysis of **1a** (at 200 °C, followed by annealing at 350 °C) resulted in the isolation of crystalline tetragonal β -Mo₂N, and investigation of the single-source CVD of MoN_x using this precursor is currently underway. Finally, the combined experimental and computational results show that rigid chelating coordinating ligands improve the overall thermal stability of the (RN)₂MoCl₂ framework by imposing a strict hexacoordinate geometry on the metal center that cannot be easily perturbed by the ligand shifting from κ_1 to κ_2 coordination geometry.

Experimental Section

Synthesis. *General Experimental.* All manipulations were performed under air-free conditions using either standard Schlenk techniques or in a nitrogen-filled (99.998% purity) MBraun glovebox. Sodium molybdate ($\geq 98\%$), triethylamine ($\geq 99\%$), chlorotrimethylsilane ($\geq 98\%$), *tert*-octylamine (95%), 1,2-dimethoxyethane ($\geq 99\%$), and *N,N,N',N'*-tetramethylethylenediamine (99%) were purchased from Sigma-Aldrich and was used as received. 2,2'-Bipyridine (98%) was purchased from Alfa Aesar and was purified by recrystallization from ethanol. (tBuN)₂MoCl₂·tmeda (**1a**),²⁸ (tPeN)₂MoCl₂·tmeda (**1b**),³⁶ (NCMe₂(CH₂)₂CMe₂N)MoCl₂·tmeda

(**1c**),³⁶ (AdN)₂MoCl₂·tmeda (**1d**),³⁶ (tBuN)₂MoCl₂·bpy (**2a**),²⁸ (tBuN)₂MoCl₂·tBu^ldad (**3**),³⁶ (tBuN)₂MoCl₂·xy^ldad (**4**),³⁶ (tBuN)₂MoCl₂·phen (**5**),³⁶ (tBuN)₂MoCl₂·impy (**6**),³⁶ (tBuN)₂MoCl₂·dmampy (**7**),³⁶ (xy^lN)₂MoCl₂·dme,⁹⁴ and 1,4-di-*tert*-butyl-1,3-diazabutadiene (tBu^ldad)⁹⁵ were all prepared following known methods. All solvents (ACS reagent-grade) were purified using a MBraun Solvent Purification System and were stored over 4 Å molecular sieves. All glassware was oven-dried at 130 °C, for at least 3 hours, prior to use. ¹H and ¹³C{¹H} NMR spectra were collected on either a Bruker AVANCE 300 MHz spectrometer or a JEOL RESONANCE ECZ400S (400 MHz) spectrometer, at room temperature and are referenced to residual solvent. C₆D₆ was purchased from Cambridge Isotope Laboratories, Inc. and was degassed using freeze-pump-thaw cycles prior to being stored over 4 Å molecular sieves, under nitrogen. Gas chromatography-mass spectrometry was performed on an Agilent Technologies 5977E GC/MSD system, at the Carleton Mass Spectrometry Centre. Elemental analyses were performed on a PerkinElmer 2400 combustion CHN analyser at the University of Windsor.

(tOctN)₂MoCl₂·dme. Prepared following a known method,⁵² with a slight modification; MoO₂Cl₂ was generated *in situ* following known protocols,^{94,96–100} instead of being prepared separately. Triethylamine (27 mL, 194 mmol), chlorotrimethylsilane (50 mL, 394 mmol), and *tert*-octylamine (16 mL, 100 mmol) were added to a suspension of sodium molybdate (10.001 g, 48.567 mmol) in 150 mL of 1,2-dimethoxyethane. The mixture was heated to 95 °C in a sealed 350-mL pressure vessel for 24 hours. The resulting dark yellow suspension was filtered through a sintered-glass frit, and the residual solids were washed with pentane until it ran clear (three, 7 mL portions). The volatiles of the filtrate were then removed *in vacuo* resulting in a dark yellow/brown oil. The oil was dissolved in 40 mL of pentane and was stored at –30 °C for 4 hours and the resulting yellow crystals were collected on a sintered-glass frit, wash with three, 10 mL portions of cold pentane,

and were dried *in vacuo* resulting in a yellow powder. Yield = 15.516 g (30.352 mmol, 62%). ^1H NMR (300 MHz, C_6D_6 , ppm): δ 1.08 (s, 18H, $\text{C}(\text{CH}_3)_3$), 1.63 (s, 12H, $\text{C}(\text{CH}_3)_2$), 1.89 (s, 4H, CH_2), 3.22 (s, 4H, OCH_2), 3.45 (s, 6H, OCH_3). $^{13}\text{C}\{^1\text{H}\}$ NMR (75 MHz, C_6D_6 , ppm): δ 30.50 ($\text{C}(\text{CH}_3)_2$), 31.47 (CH_2), 31.95 ($\text{C}(\text{CH}_3)_3$), 55.45 ($\text{C}(\text{CH}_3)_3$), 62.16 (OCH_2), 70.83 (OCH_3), 76.28 ($\text{C}(\text{CH}_3)_2$). Selected IR data (KBr, cm^{-1}): $\nu(\text{Mo}=\text{N})$ 1222 (s), 1242 (m).

($^t\text{OctN}$) $_2\text{MoCl}_2\cdot\text{tmeda}$ (**1e**). *N,N,N'N'*-Tetramethylethylenediamine (0.9 mL, 6.0 mmol) was added to a solution of ($^t\text{OctN}$) $_2\text{MoCl}_2\cdot\text{dme}$ (2.151 g, 4.208 mmol) in 40 mL of diethyl ether. After stirring at room temperature for 2 hours the volatiles were removed *in vacuo* resulting in a waxy orange solid. The solid was dissolved in 8 mL of benzene which was subsequently frozen in liquid nitrogen, and removed by sublimation (lyophilization), resulting in a pale-orange powder. Yield = 2.038 g (4.002 mmol, 95%). X-ray quality crystals were obtained after storing a concentrated pentane solution at $-30\text{ }^\circ\text{C}$ for 3 days. ^1H NMR (400 MHz, C_6D_6 , ppm): δ 1.05 (s, 18H, $\text{C}(\text{CH}_3)_3$), 1.61 (s, 12H, $(\text{CH}_3)_2$), 2.05 (s, 4H, CH_2), 2.09 (s, 4H, NCH_2), 2.59 (s, 12H, $\text{N}(\text{CH}_3)_2$). $^{13}\text{C}\{^1\text{H}\}$ NMR (100 MHz, C_6D_6 , ppm): δ 29.82 ($\text{C}(\text{CH}_3)_2$), 31.49 (CH_2), 31.97 ($\text{C}(\text{CH}_3)_3$), 50.63 ($\text{N}(\text{CH}_3)_2$), 55.04 ($\text{C}(\text{CH}_3)_3$), 57.30 (NCH_2), 75.99 ($\text{C}(\text{CH}_3)_2$). Selected IR data (KBr, cm^{-1}): $\nu(\text{Mo}=\text{N})$ 1213 (vs), 1242 (s). EA calcd for $\text{C}_{22}\text{H}_{50}\text{Cl}_2\text{MoN}_4$ [%]: C, 49.16; H, 9.38; N, 10.42; found [%]: C, 49.28; H, 9.58; N, 10.10.

($^t\text{OctN}$) $_2\text{MoCl}_2\cdot\text{bpy}$ (**2e**). 2,2'-Bipyridine (0.414 g, 2.651 mmol) was added to a solution of ($^t\text{OctN}$) $_2\text{MoCl}_2\cdot\text{dme}$ (1.216 g, 2.379 mmol) in 20 mL of diethyl ether. After stirring at room temperature for 2 hours the mixture was filtered through a sintered glass frit, and an orange solid was collected. The solid was washed with two, 3 mL portions of diethyl ether, and three, 3 mL portions of pentane. The solids were dried *in vacuo* resulting in an analytically pure pale-orange powder. Yield = 1.294 g (2.241 mmol, 94%). X-ray quality crystals were obtained after storing a

concentrated dichloromethane solution, layered with pentane, at $-30\text{ }^{\circ}\text{C}$ for 5 hours. ^1H NMR (400 MHz, C_6D_6 , ppm): δ 1.21 (s, 18H, $\text{C}(\text{CH}_3)_3$), 1.90 (s, 12H, $(\text{CH}_3)_2$), 2.22 (s, 4H, CH_2), 6.70 (t, 2H, $J = 6.0$ Hz), 6.91 (td, 2H, $J = 8.0$ & 1.6 Hz), 7.07 (d, 2H, $J = 8.0$ Hz), 9.63 (d, 2H, $J = 4.8$ Hz). $^{13}\text{C}\{^1\text{H}\}$ NMR (100 MHz, C_6D_6 , ppm): δ 31.06 ($\text{C}(\text{CH}_3)_2$), 31.61 (CH_2), 32.24 ($\text{C}(\text{CH}_3)_3$), 56.38 ($\text{C}(\text{CH}_3)_3$), 75.71 ($\text{C}(\text{CH}_3)_2$), 121.63, 124.57, 138.02, 150.81, 152.78. Selected IR data (KBr, cm^{-1}): $\nu(\text{Mo}=\text{N})$ 1223 (s), 1240 (m). EA calcd for $\text{C}_{26}\text{H}_{42}\text{Cl}_2\text{MoN}_4$ [%]: C, 54.08; H, 7.33; N, 9.70; found [%]: C, 53.72; H, 7.19; N, 9.62.

$[(^t\text{OctN})_2\text{Mo}(\mu\text{-Cl})_2]_{\infty}(\text{Oe})_{\infty}$. $(^t\text{OctN})_2\text{MoCl}_2\cdot\text{dme}$ (1.138 g, 2.225 mmol) was sublimed under dynamic vacuum ($120\text{ }^{\circ}\text{C}$, 40 mTorr) over two hours onto a water-cooled cold finger resulting in a pale-orange powder. Yield = 0.838 g (0.995 mmol, 89% based on Mo). X-ray quality crystals were obtained after storing a concentrated toluene solution at $-30\text{ }^{\circ}\text{C}$ for 2 weeks. ^1H NMR (400 MHz, C_6D_6 , ppm): δ 1.07 (s, 36H, $\text{C}(\text{CH}_3)_3$), 1.47 (s, 24H, $(\text{CH}_3)_2$), 1.57 (s, 8H, CH_2). $^{13}\text{C}\{^1\text{H}\}$ NMR (100 MHz, C_6D_6 , ppm): δ 31.39 ($\text{C}(\text{CH}_3)_2$), 31.71 (CH_2), 31.80 ($\text{C}(\text{CH}_3)_3$), 55.08 ($\text{C}(\text{CH}_3)_3$), 78.12 ($\text{C}(\text{CH}_3)_2$). Selected IR data (KBr, cm^{-1}): $\nu(\text{Mo}=\text{N})$ 1208 (s), 1231 (m). EA calcd for $\text{C}_{32}\text{H}_{68}\text{Cl}_4\text{Mo}_2\text{N}_4$ [%]: C, 45.61; H, 8.13; N, 6.65; found [%]: C, 45.32; H, 8.29; N, 7.32.

Thermal Characterization. *In Situ Thermolysis Reactions.* The analyte of study was dissolved in C_6D_6 , in a thick-walled NMR tube. The solution was frozen in liquid nitrogen and the NMR tube was flame-sealed under vacuum and was stored at room temperature for 18 hours to ensure stoichiometry and stability. For the thermolysis reactions, the flame-sealed NMR tubes were stored in an oven with an internal temperature of $185\text{ }^{\circ}\text{C}$ for several days, with ^1H NMR spectra collected at varying intervals.

Neat Thermolysis Reactions. The solid compound (0.413 g of **1a**, or 0.808 g of **1e**) was placed inside a 50 mL Schlenk tube and was placed under static vacuum (40 mTorr). The flask was then

thoroughly heated with a heat gun (*ca.* 200 °C), ensuring the entire flask was heated to prevent sublimation. The compound gradually darkened, eventually resulting in a black residue, forming a metallic-like film on the inside of the flask (Figure S17). After the thermolysis, a receiving flask, cooled in liquid nitrogen, was attached to the first flask, and the volatile byproducts were collected, resulting in a clear and colorless liquid. The liquid was analyzed by ¹H NMR spectroscopy and GC-MS, and the dark residue was analyzed by TEM/EDS. Some of the dark residue was also annealed at 350 °C for 15 minutes, under nitrogen, using the furnace on a TGA instrument.

Thermogravimetric Analysis. TGA was performed on a TA Instruments Discovery TGA 55 instrument which was housed in a “chemical-free”, nitrogen-filled (99.998%) MBraun Labmaster 130 glovebox. In a typical experiment 10.000 ± 0.100 mg of analyte was placed in a platinum pan and was heated to 500 °C with a ramp rate of 10 °C min⁻¹, unless otherwise stated, using nitrogen (99.999% purity, 60 sccm) as the purge gas. Platinum pans were cleaned by sequential sonication in glacial acetic acid then isopropanol, followed by heating until red-hot with a propane torch. Langmuir vapor pressure equations were derived from TGA data using a previously reported method, employing benzoic acid as the calibrant.^{101,102}

Differential Scanning Calorimetry. DSC experiments were performed with a TA Instruments Q10 instrument. The DSC was calibrated at the melting point of indium metal (156.6 °C). All DSC samples were hermetically sealed in aluminum pans inside a glovebox prior to analysis. All samples were heated to 400 °C with a ramp rate of 10 °C min⁻¹, using nitrogen (99.998% purity, 50 sccm) as the purge gas.

High-Resolution Mass Spectrometry. High-resolution mass spectra were collected on a Kratos Concept electron impact mass spectrometer, at the John L. Holmes Mass Spectrometry Facility at the University of Ottawa. The spectra were collected by direct injection, of a glass capillary filled

with the analyte, with a source temperature of 250 °C, and using perfluorokerosene as an internal calibrant.

Transmission Electron Microscopy. TEM measurements were performed on a FEI Tecnai G2 F20 Transmission Electron Microscope equipped with an Oxford AztecTEM SDD detector. Samples for analysis were prepared by drop casting a suspension of the residue in pentane onto a copper TEM grid, which was subsequently dried *in vacuo*.

X-Ray Crystallography. The crystallographic diagrams were prepared using ORTEP-3 for Windows.¹⁰³ Specific details about data collection and refinements can be found in the Supporting Information.

Quantum Chemical Calculations. All calculations were carried out with ORCA 5.0.2 using default settings (i.e., grid sizes, convergence, etc.).¹⁰⁴ Guess geometries were either extracted from single-crystal X-ray diffraction structures or drawn by hand in Avogadro 1.2.0.¹⁰⁵ Geometry optimizations and analytic frequency calculations were performed with the composite density functional theory (DFT) method r²SCAN-3c⁸⁹ which combines the r²SCAN meta-generalized gradient approximation (mGGA) exchange-correlation functional,¹⁰⁶ refitted charge-dependent D4 London dispersion correction,¹⁰⁶⁻¹⁰⁸ geometric counter-poise (gCP) basis set superposition error (BSSE) correction,^{106,109} and the def2-mTZVPP atomic orbital basis set. Minimum energy pathways (MEPs) were found using the climbing image nudged elastic band method (CI-NEB) with twelve (12) images between the previously optimized minima and a subsequent full eigenvector-following optimization starting from the climbing image to find the true saddle point (NEB-TS).⁹⁰ Stationary points were confirmed to have all real frequencies while saddle points were confirmed to have exactly one imaginary frequency, and all thermodynamic quantities were calculated using default settings under standard conditions. Saddle points were confirmed to

connect the expected products to reactants by intrinsic reaction coordinate (IRC) analysis. Geometries for the high energy four-membered cyclic transition states to form the hydrogen-terminated imido Mo(VI) complex for either of the *tert*-butyl groups on the dimer (**0a**)₂ would not converge with the r2SCAN-3c method, but they were found during a preliminary study using ORCA 4.2.1 with default settings, revPBE exchange-correlation functional,¹¹⁰ Grimme's empirical atom-pairwise dispersion correction with Becke-Johnson damping [D3(BJ)],^{111,112} Karlsruhe basis sets¹¹³ of double-zeta quality (def2-SVP) on all elements except triple-zeta quality with polarization (def2-TZVPP) with a 28-electron effective core potential (ECP-28) on molybdenum (Mo).¹¹⁴ Final single-point energy calculations were performed on all optimized structures using the domain-based local pair natural orbital coupled cluster theory with singles, doubles, and perturbative triples [DLPNO-CCSD(T)]^{91,92} method with NormalPNO settings and a triple-zeta quality basis set with polarization (def2-TZVPP) on all atoms and a 28-electron effective core potential (ECP-28) on molybdenum (Mo).¹¹⁴ The mean absolute deviation (MAD) between the r²SCAN-3c and DLPNO-CCSD(T) calculations for the reaction and barrier energies was 3.36 kcal·mol⁻¹. Illustrations of the calculated geometries were rendered procedurally with Jmol¹¹⁵ or by-hand with UCSF Chimera.¹¹⁶

Associated Content

Supporting Information

The Supporting Information is available free of charge on the ACS Publications website at DOI:

NMR and IR spectra; *in situ* and solid-state thermolysis reactions; EI-HRMS analysis; TGA plots; DSC curves; crystallographic information files for all compounds deposited at the CCDC (2164483-2164486) (PDF). Cartesian coordinates and images of all optimized structures; trajectories and movies of all IRC pathways; calculated electronic energies, thermodynamic corrections, and reaction energies (ZIP).

Author Information

Corresponding Author

*E-mail: Michael.land@carleton.ca

ORCID

Michael A. Land: 0000-0001-5861-242X

Goran Bačić: 0000-0003-2437-2418

Katherine N. Robertson: 0000-0002-5602-8059

Seán T. Barry: 0000-0001-5515-4734

Author Contributions

The manuscript was written through contributions of all authors. All authors have given approval to the final version of the manuscript.

Acknowledgements

M.A.L. thanks the Natural Sciences and Engineering Council of Canada (NSERC) for funding through the Alexander Graham Bell CGS-D Scholarship. S.T.B. acknowledges NSERC for support through the Discovery Grants Program (RGPIN-2019-06213). We also thank Jianqun Wang and Karl Wasslen from Carleton University for TEM and GC-MS acquisition, Sharon Curtis from the University of Ottawa for HRMS acquisition, and Lara Watanabe from the University of

Windsor for EA acquisition. Finally, we thank the Digital Research Alliance of Canada for computation time on the Cedar cluster.

References

- (1) Wright, W. R. H.; Batsanov, A. S.; Messinis, A. M.; Howard, J. A. K.; Tooze, R. P.; Hanton, M. J.; Dyer, P. W. Application of Molybdenum Bis(Imido) Complexes in Ethylene Dimerisation Catalysis. *Dalton Trans.* **2012**, 41 (18), 5502.
- (2) Schrock, R. Recent Advances in Olefin Metathesis by Molybdenum and Tungsten Imido Alkylidene Complexes. *J. Mol. Catal. A Chem.* **2004**, 213 (1), 21–30.
- (3) Liu, S.; Amaro-Estrada, J. I.; Baltrun, M.; Douair, I.; Schoch, R.; Maron, L.; Hohloch, S. Catalytic Deoxygenation of Nitroarenes Mediated by High-Valent Molybdenum(VI)–NHC Complexes. *Organometallics* **2021**, 40 (2), 107–118.
- (4) Mösch-Zanetti, N. C.; Wurm, D.; Volpe, M.; Lyashenko, G.; Harum, B.; Belaj, F.; Baumgartner, J. Replacement of an Oxo by an Imido Group in Oxotransferase Model Compounds: Influence on the Oxygen Atom Transfer. *Inorg. Chem.* **2010**, 49 (19), 8914–8921.
- (5) Zwettler, N.; Grover, N.; Belaj, F.; Kirchner, K.; Mösch-Zanetti, N. C. Activation of Molecular Oxygen by a Molybdenum(IV) Imido Compound. *Inorg. Chem.* **2017**, 56 (17), 10147–10150.
- (6) Hüttinger, K.; Förster, C.; Bund, T.; Hinderberger, D.; Heinze, K. Stereochemical Consequences of Oxygen Atom Transfer and Electron Transfer in Imido/Oxido

- Molybdenum(IV, V, VI) Complexes with Two Unsymmetric Bidentate Ligands. *Inorg. Chem.* **2012**, *51* (7), 4180–4192.
- (7) Chiu, H.-T.; Chang, G.-B.; Ho, W.-Y.; Chuang, S.-H.; Lee, G.-H.; Peng, S.-M. Syntheses and X-Ray Crystal Structures of Dichlorobis(Tert-Butylimido) Complexes of Molybdenum(VI); Potential Precursors to Molybdenum Nitride and Molybdenum Carbonitride. *J. Chinese Chem. Soc.* **1994**, *41* (6), 755–761.
- (8) Chiu, H. T.; Ho, W. Y.; Chuang, S. H. Deposition of Molybdenum Carbonitride Thin Films from Mo(NBut)₂(NHBut)₂. *J. Mater. Res.* **1994**, *9* (7), 1622–1624.
- (9) Gwildies, V.; Thiede, T. B.; Amirjalayer, S.; Alsamman, L.; Devi, A.; Fischer, R. A. All-Nitrogen Coordinated Amidinato/Imido Complexes of Molybdenum and Tungsten: Syntheses and Characterization. *Inorg. Chem.* **2010**, *49* (18), 8487–8494.
- (10) Srinivasan, N. B.; Thiede, T. B.; de los Arcos, T.; Gwildies, V.; Krasnopolski, M.; Becker, H. W.; Rogalla, D.; Devi, A.; Fischer, R. A. Transition Metal Nitride Thin Films Grown by MOCVD Using Amidinato Based Complexes [M(NtBu)₂{(IPrN)₂CMe₂}₂] (M=Mo, W) as Precursors. *Surf. Coatings Technol.* **2013**, *230*, 130–136.
- (11) Bertuch, A.; Sundaram, G.; Saly, M.; Moser, D.; Kanjolia, R. Atomic Layer Deposition of Molybdenum Oxide Using Bis(Tert-Butylimido)Bis(Dimethylamido) Molybdenum. *J. Vac. Sci. Technol. A Vacuum, Surfaces, Film.* **2014**, *32* (1), 01A119.
- (12) Ziegler, J.; Mews, M.; Kaufmann, K.; Schneider, T.; Sprafke, A. N.; Korte, L.; Wehrspohn, R. B. Plasma-Enhanced Atomic-Layer-Deposited MoO_x Emitters for Silicon Heterojunction Solar Cells. *Appl. Phys. A* **2015**, *120* (3), 811–816.

- (13) Macco, B.; Vos, M. F. J.; Thissen, N. F. W.; Bol, A. A.; Kessels, W. M. M. Low-Temperature Atomic Layer Deposition of MoO_x for Silicon Heterojunction Solar Cells. *Phys. status solidi - Rapid Res. Lett.* **2015**, *9* (7), 393–396.
- (14) Vos, M. F. J.; Macco, B.; Thissen, N. F. W.; Bol, A. A.; Kessels, W. M. M. (Erwin). Atomic Layer Deposition of Molybdenum Oxide from (N t Bu)₂ (NMe₂)₂ Mo and O₂ Plasma. *J. Vac. Sci. Technol. A Vacuum, Surfaces, Film.* **2016**, *34* (1), 01A103.
- (15) Jang, Y.; Kim, J. B.; Hong, T. E.; Yeo, S. J.; Lee, S.; Jung, E. A.; Park, B. K.; Chung, T. M.; Kim, C. G.; Lee, D. J.; Lee, H. B. R.; Kim, S. H. Highly-Conformal Nanocrystalline Molybdenum Nitride Thin Films by Atomic Layer Deposition as a Diffusion Barrier against Cu. *J. Alloys Compd.* **2016**, *663*, 651–658.
- (16) Bertuch, A.; Keller, B. D.; Ferralis, N.; Grossman, J. C.; Sundaram, G. Plasma Enhanced Atomic Layer Deposition of Molybdenum Carbide and Nitride with Bis(Tert - Butylimido)Bis(Dimethylamido) Molybdenum. *J. Vac. Sci. Technol. A Vacuum, Surfaces, Film.* **2017**, *35* (1), 01B141.
- (17) Keller, B. D.; Bertuch, A.; Provine, J.; Sundaram, G.; Ferralis, N.; Grossman, J. C. Process Control of Atomic Layer Deposition Molybdenum Oxide Nucleation and Sulfidation to Large-Area MoS₂ Monolayers. *Chem. Mater.* **2017**, *29* (5), 2024–2032.
- (18) Cwik, S.; Mitoraj, D.; Mendoza Reyes, O.; Rogalla, D.; Peeters, D.; Kim, J.; Schütz, H. M.; Bock, C.; Beranek, R.; Devi, A. Direct Growth of MoS₂ and WS₂ Layers by Metal Organic Chemical Vapor Deposition. *Adv. Mater. Interfaces* **2018**, *5* (16), 1–11.
- (19) Sun, S.-C.; Chiu, H.-T. MOCVD Molybdenum Nitride Diffusion Barrier for Cu

- Metallization. US6114242A, 2000.
- (20) Mattinen, M.; Wree, J. L.; Stegmann, N.; Ciftiyurek, E.; Achhab, M. El; King, P. J.; Mizohata, K.; Räisänen, J.; Schierbaum, K. D.; Devi, A.; Ritala, M.; Leskelä, M. Atomic Layer Deposition of Molybdenum and Tungsten Oxide Thin Films Using Heteroleptic Imido-Amidinato Precursors: Process Development, Film Characterization, and Gas Sensing Properties. *Chem. Mater.* **2018**, *30* (23), 8690–8701.
- (21) Sharma, A.; Verheijen, M. A.; Wu, L.; Karwal, S.; Vandalon, V.; Knoop, H. C. M.; Sundaram, R. S.; Hofmann, J. P.; Kessels, W. M. M.; Bol, A. A. Low-Temperature Plasma-Enhanced Atomic Layer Deposition of 2-D MoS₂: Large Area, Thickness Control and Tuneable Morphology. *Nanoscale* **2018**, *10* (18), 8615–8627.
- (22) Xu, H.; Akbari, M. K.; Hai, Z.; Wei, Z.; Hyde, L.; Verpoort, F.; Xue, C.; Zhuiykov, S. Ultra-Thin MoO₃ Film Goes Wafer-Scaled Nano-Architectonics by Atomic Layer Deposition. *Mater. Des.* **2018**, *149*, 135–144.
- (23) Wei, Z.; Hai, Z.; Akbari, M. K.; Qi, D.; Xing, K.; Zhao, Q.; Verpoort, F.; Hu, J.; Hyde, L.; Zhuiykov, S. Atomic Layer Deposition-Developed Two-Dimensional α -MoO₃ Windows Excellent Hydrogen Peroxide Electrochemical Sensing Capabilities. *Sensors Actuators B Chem.* **2018**, *262*, 334–344.
- (24) Cho, Y. K.; Choi, Y.; Kim, S.-G.; Jun, Y.; Kim, H. Influence of Hydrogen Supply on Mo(C,N) Films Synthesized by Plasma-Enhanced Chemical Vapor Deposition Using Bis(Tert-butylimido) Bis(Dimethylamido) Molybdenum. *Thin Solid Films* **2019**, *692* (December 2018), 137607.

- (25) Sopha, H.; Tesfaye, A. T.; Zazpe, R.; Michalicka, J.; Dvorak, F.; Hromadko, L.; Krbal, M.; Prikryl, J.; Djenizian, T.; Macak, J. M. ALD Growth of MoS₂ Nanosheets on TiO₂ Nanotube Supports. *FlatChem* **2019**, *17*, 100130.
- (26) Kalanyan, B.; Beams, R.; Katz, M. B.; Davydov, A. V.; Maslar, J. E.; Kanjolia, R. K. MoS₂ Thin Films from a (N t Bu)₂ (NMe₂)₂ Mo and 1-Propanethiol Atomic Layer Deposition Process. *J. Vac. Sci. Technol. A* **2019**, *37* (1), 010901.
- (27) Mughal, A. J.; Walter, T. N.; Cooley, K. A.; Bertuch, A.; Mohny, S. E. Effect of Substrate on the Growth and Properties of MoS₂ Thin Films Grown by Plasma-Enhanced Atomic Layer Deposition. *J. Vac. Sci. Technol. A* **2019**, *37* (1), 010907.
- (28) Land, M. A.; Robertson, K. N.; Barry, S. T. Ligand-Assisted Volatilization and Thermal Stability of Bis(Imido)Dichloromolybdenum(VI) ((t-BuN=)₂MoCl₂)₂ and Its Adducts. *Organometallics* **2020**, *39* (7), 916–927.
- (29) Ou, N. C.; Preradovic, K.; Ferenczy, E. T.; Sparrow, C. B.; Germaine, I. M.; Jurca, T.; Craciun, V.; Mcelwee-White, L. Synthesis and Evaluation of Molybdenum Imido-Thiolato Complexes for the Aerosol-Assisted Chemical Vapor Deposition of Nitrogen-Doped Molybdenum Disulfide. *Organometallics* **2020**, *39* (7), 956–966.
- (30) Dezelah IV, C. L.; El-Kadri, O. M.; Heeg, M. J.; Winter, C. H. Preparation and Characterization of Molybdenum and Tungsten Nitride Nanoparticles Obtained by Thermolysis of Molecular Precursors. *J. Mater. Chem.* **2004**, *14* (21), 3167–3176.
- (31) Wree, J. L.; Ciftyurek, E.; Zanders, D.; Boysen, N.; Kostka, A.; Rogalla, D.; Kasischke, M.; Ostendorf, A.; Schierbaum, K.; Devi, A. A New Metalorganic Chemical Vapor Deposition

- Process for MoS₂ with a 1,4-Diazabutadienyl Stabilized Molybdenum Precursor and Elemental Sulfur. *Dalton Trans.* **2020**, 49 (38), 13462–13474.
- (32) Vandalon, V.; Bol, A. A.; Verheijen, M. A.; Kessels, W. M. M. Atomic Layer Deposition of Al-Doped MoS₂: Synthesizing a p-Type 2D Semiconductor with Tunable Carrier Density. *ACS Appl. Nano Mater.* **2020**, 3 (10), 10200–10208.
- (33) Shen, C.; Raza, M. H.; Amsalem, P.; Schultz, T.; Koch, N.; Pinna, N. Morphology-Controlled MoS₂ by Low-Temperature Atomic Layer Deposition. *Nanoscale* **2020**, 12 (39), 20404–20412.
- (34) Chowdhury, M. I.; Sowa, M.; Kozen, A. C.; Krick, B. A.; Haik, J.; Babuska, T. F.; Strandwitz, N. C. Plasma Enhanced Atomic Layer Deposition of Titanium Nitride-Molybdenum Nitride Solid Solutions. *J. Vac. Sci. Technol. A* **2021**, 39 (1), 012407.
- (35) Molina, A.; Campbell, I. E.; Walter, T. N.; Agyapong, A. D.; Mohny, S. E. Molybdenum Carbonitride Deposited by Plasma Atomic Layer Deposition as a Schottky Contact to Gallium Nitride. *Appl. Phys. Lett.* **2021**, 119 (10), 102102.
- (36) Land, M. A.; Bačić, G.; Robertson, K. N.; Barry, S. T. Thermal Stability and Decomposition Pathways in Volatile Molybdenum(VI) Bis-Imides. *Inorg. Chem.* **2022**, 61 (12), 4980–4994.
- (37) Miikkulainen, V.; Suvanto, M.; Pakkanen, T. A. Atomic Layer Deposition of Molybdenum Nitride from Bis(Tert -Butylimido)-Bis(Dimethylamido)Molybdenum and Ammonia onto Several Types of Substrate Materials with Equal Growth per Cycle. *Chem. Mater.* **2007**, 19 (2), 263–269.

- (38) Miikkulainen, V.; Suvanto, M.; Pakkanen, T. A. Bis(Tert-Butylimido)-Bis(Dialkylamido) Complexes of Molybdenum as Atomic Layer Deposition (ALD) Precursors for Molybdenum Nitride: The Effect of the Alkyl Group. *Chem. Vap. Depos.* **2008**, *14* (3–4), 71–77.
- (39) Miikkulainen, V.; Suvanto, M.; Pakkanen, T. A. Molybdenum Nitride Nanotubes. *Thin Solid Films* **2008**, *516* (18), 6041–6047.
- (40) Miikkulainen, V.; Suvanto, M.; Pakkanen, T. A.; Siitonen, S.; Karvinen, P.; Kuittinen, M.; Kisonen, H. Thin Films of MoN, WN, and Perfluorinated Silane Deposited from Dimethylamido Precursors as Contamination Resistant Coatings on Micro-Injection Mold Inserts. *Surf. Coatings Technol.* **2008**, *202* (21), 5103–5109.
- (41) Rische, D. MOCVD of Tungsten and Molybdenum Nitrides, 2007.
- (42) Thiede, T.; Gwildies, V.; Alsamann, L.; Rische, D.; Fischer, R. Novel Precursors for the MOCVD of Molybdenum Nitride. In *ECS Transactions*; ECS, 2009; Vol. 25, pp 593–600.
- (43) Coyle, J. P.; Kurek, A.; Pallister, P. J.; Sirianni, E. R.; Yap, G. P. A.; Barry, S. T. Preventing Thermolysis: Precursor Design for Volatile Copper Compounds. *Chem. Commun.* **2012**, *48* (84), 10440.
- (44) Barry, S. T. Amidinates, Guanidates and Iminopyrrolidates: Understanding Precursor Thermolysis to Design a Better Ligand. *Coord. Chem. Rev.* **2013**, *257* (23–24), 3192–3201.
- (45) Wu, J.; Li, J.; Zhou, C.; Lei, X.; Gaffney, T.; Norman, J. A. T.; Li, Z.; Gordon, R.; Cheng, H. Computational Study on the Relative Reactivities of Cobalt and Nickel Amidinates via

- β -H Migration. *Organometallics* **2007**, 26 (11), 2803–2805.
- (46) Li, Z.; Gordon, R. G.; Pallem, V.; Li, H.; Shenai, D. V. Direct-Liquid-Injection Chemical Vapor Deposition of Nickel Nitride Films and Their Reduction to Nickel Films. *Chem. Mater.* **2010**, 22 (10), 3060–3066.
- (47) Beh, E. S.; Tong, L.; Gordon, R. G. Synthesis of 5,5-Bicyclic Amidines as Ligands for Thermally Stable Vapor Deposition Precursors. *Organometallics* **2017**, 36 (8), 1453–1456.
- (48) Barry, S. T. *Chemistry of Atomic Layer Deposition*; De Gruyter: Berlin, Boston, 2021.
- (49) Mouat, A. R.; Mane, A. U.; Elam, J. W.; Delferro, M.; Marks, T. J.; Stair, P. C. Volatile Hexavalent Oxo-Amidinate Complexes: Molybdenum and Tungsten Precursors for Atomic Layer Deposition. *Chem. Mater.* **2016**, 28 (6), 1907–1919.
- (50) Mukhopadhyay, A. B.; Musgrave, C. B. The Role of Ammonia in Atomic Layer Deposition of Tungsten Nitride. *Appl. Phys. Lett.* **2007**, 90 (17), 2005–2008.
- (51) Miikkulainen, V.; Suvanto, M.; Pakkanen, T. A. Atomic Layer Deposition of Molybdenum Nitride from Bis(Tert-Butylimido)- Bis(Dimethylamido)Molybdenum and Ammonia onto Several Types of Substrate Materials with Equal Growth per Cycle. *Chem. Mater.* **2007**, 19 (2), 263–269.
- (52) Migdal, C. A.; Stott, P. E.; Ustynyuk, N. A.; Zaroubine, D. N.; Yampolsky, I. V.; Rufanov, K. . A. Organomolybdenum Complexes as Friction Modifiers. WO2003008428A1, 2003.
- (53) Parkin, G.; Van Asselt, A.; Leahy, D. J.; Whinnery, L.; Hua, N. G.; Quan, R. W.; Henling, L. M.; Schaefer, W. P.; Santarsiero, B. D.; Bercaw, J. E. Oxo-Hydrido and Imido-Hydrido

- Derivatives of Permethyltantalocene. Structures of (.Eta.5-C5Me5)2Ta(:O)H and (.Eta.5-C5Me5)2Ta(:NC6H5)H: Doubly or Triply Bonded Tantalum Oxo and Imido Ligands? *Inorg. Chem.* **1992**, *31* (1), 82–85.
- (54) Barrie, P.; Coffey, T. A.; Forster, G. D.; Hogarth, G. Bent vs. Linear Imido Ligation at the Octahedral Molybdenum(VI) Dithiocarbamate Stabilised Centre. *J. Chem. Soc. Dalton Trans.* **1999**, No. 24, 4519–4528.
- (55) Siemeling, U.; Türk, T.; Schoeller, W. W.; Redshaw, C.; Gibson, V. C. Benefits of the Chelate Effect: Preparation of an Unsymmetrical Ansa -Bis(Imido)Molybdenum Complex Containing a Seven-Membered Chelate Ring . *Inorg. Chem.* **1998**, *37* (18), 4738–4739.
- (56) Ciszewski, J. T.; Harrison, J. F.; Odom, A. L. Investigation of Transition Metal–Imido Bonding in M(NBu t) 2 (Dpma). *Inorg. Chem.* **2004**, *43* (12), 3605–3617.
- (57) Falivene, L.; Cao, Z.; Petta, A.; Serra, L.; Poater, A.; Oliva, R.; Scarano, V.; Cavallo, L. Towards the Online Computer-Aided Design of Catalytic Pockets. *Nat. Chem.* **2019**, *11* (10), 872–879.
- (58) Groom, C. R.; Bruno, I. J.; Lightfoot, M. P.; Ward, S. C. The Cambridge Structural Database. *Acta Crystallogr. Sect. B Struct. Sci. Cryst. Eng. Mater.* **2016**, *72* (2), 171–179.
- (59) Griffith, W. .; Skapski, A. .; Woode, K. .; Wright, M. . Partial Coordination in Amine Adducts of Osmium Tetraoxide: X-Ray Molecular Structure of Quinuclidinetetraoxo-Osmium(VIII). *Inorganica Chim. Acta* **1978**, *31*, L413–L414.
- (60) Heeg, M. J.; Williams, D. S.; Elgammal, R. CSD NAWTOV. *14* (14), 10–12.

- (61) Borjas Nevarez, R.; Balasekaran, S. M.; Kim, E.; Weck, P.; Poineau, F. Zirconium Tetrachloride Revisited. *Acta Crystallogr. Sect. C Struct. Chem.* **2018**, *74* (3), 307–311.
- (62) Wu, J.-B.; Yang, Y.; Lin, Y.-F.; Chiu, H.-T. Surface Reaction of Bis(Tertbutylimido)Bis(Diethylamido)Tungsten Precursor on Si(100)–(2×1). *J. Vac. Sci. Technol. A Vacuum, Surfaces, Film.* **2003**, *21* (5), 1620–1624.
- (63) Crane, E. L.; Chiu, H.-T.; Nuzzo, R. G. Kinetic and Mechanistic Studies of the Chemical Vapor Deposition of Tungsten Nitride from Bis(Tertbutylimido)Bis(Tertbutylamido)Tungsten. *J. Phys. Chem. B* **2001**, *105* (17), 3549–3556.
- (64) Jayaratne, K. C.; Yap, G. P. A.; Haggerty, B. S.; Rheingold, A. L.; Winter, C. H. Imido Complexes Derived from the Reactions of Niobium and Tantalum Pentachlorides with Primary Amines: Relevance to the Chemical Vapor Deposition of Metal Nitride Films. *Inorg. Chem.* **1996**, *35* (17), 4910–4920.
- (65) Henderson, R. A. Mechanism of the Base-Catalysed Substitution of Halide for Methoxide in the Reactions of Trans-[W(NH)X(Ph₂PCH₂CH₂PPh₂)₂]⁺(X = Cl, Br, or I). *J. Chem. Soc. Dalton Trans.* **1983**, No. 1, 51.
- (66) Baltrun, M.; Watt, F. A.; Schoch, R.; Hohloch, S. Dioxo-, Oxo-Imido-, and Bis-Imido-Molybdenum(VI) Complexes with a Bis-Phenolate-NHC Ligand. *Organometallics* **2019**, *38* (19), 3719–3729.
- (67) Margulieux, G. W.; Kim, S.; Chirik, P. J. Determination of the N-H Bond Dissociation Free Energy in a Pyridine(Diimine)Molybdenum Complex Prepared by Proton-Coupled Electron

- Transfer. *Inorg. Chem.* **2020**, *59* (20), 15394–15401.
- (68) SDBSWeb : <https://Sdbs.Db.Aist.Go.Jp> (National Institute of Advanced Industrial Science and Technology, March 27, 2022).
- (69) Buchanan, G. L. Bredt's Rule. *Chem. Soc. Rev.* **1974**, *3* (1), 41.
- (70) Grant, D.; McKervey, M. A.; Rooney, J. J.; Samman, N. G.; Step, G. Adamantene and Its Dimer. *J. Chem. Soc., Chem. Commun.* **1972**, No. 21, 1186.
- (71) Section 3: Physical Constants of Organic Compounds. In *CRC Handbook of Chemistry and Physics*; Lide, D. R., Ed.; CRC Press: Boca Raton, FL, 2005.
- (72) Jain, A.; Ong, S. P.; Hautier, G.; Chen, W.; Richards, W. D.; Dacek, S.; Cholia, S.; Gunter, D.; Skinner, D.; Ceder, G.; Persson, K. A. Commentary: The Materials Project: A Materials Genome Approach to Accelerating Materials Innovation. *APL Mater.* **2013**, *1* (1), 011002.
- (73) Jeong, H.; Schrock, R. R.; Müller, P. Synthesis of Molybdenum and Tungsten Alkylidene Complexes That Contain a Tert-Butylimido Ligand. *Organometallics* **2015**, *34* (17), 4408–4418.
- (74) Ortiz, C. G.; Abboud, K. A.; Boncella, J. M. Synthesis of Chelate-Supported Dialkyl and Alkylidene Complexes of Molybdenum(VI). *Organometallics* **1999**, *18* (21), 4253–4260.
- (75) Potts, S. E.; Carmalt, C. J.; Blackman, C. S.; Leese, T.; Davies, H. O. Tungsten Imido Complexes as Precursors to Tungsten Carbonitride Thin Films. *Dalton Trans.* **2008**, *2* (42), 5730–5736.
- (76) Bleau, J. E.; Carmalt, C. J.; O'Neill, S. A.; Parkin, I. P.; White, A. J. P.; Williams, D. J.

- Molecular Precursors for the CVD of Niobium and Tantalum Nitride. *Polyhedron* **2005**, *24* (3), 463–468.
- (77) Carmalt, C. J.; Newport, A.; Parkin, I. P.; Mountford, P.; Sealey, A. J.; Dubberley, S. R. Synthesis of TiN Thin Films from Titanium Imido Complexes. *J. Mater. Chem.* **2003**, *13* (1), 84–87.
- (78) Bchir, O. J.; Green, K. M.; Hlad, M. S.; Anderson, T. J.; Brooks, B. C.; Wilder, C. B.; Powell, D. H.; McElwee-White, L. $\text{Cl}_4(\text{PhCN})\text{W}(\text{NPh})$ as a Single-Source MOCVD Precursor for Deposition of Tungsten Nitride (WN_x) Thin Films. *J. Organomet. Chem.* **2003**, *684* (1–2), 338–350.
- (79) Bchir, O. J.; Green, K. M.; Ajmera, H. M.; Zapp, E. A.; Anderson, T. J.; Brooks, B. C.; Reitfort, L. L.; Powell, D. H.; Abboud, K. A.; McElwee-White, L. Tungsten Allylimido Complexes $\text{Cl}_4(\text{RCN})\text{W}(\text{NC}_3\text{H}_5)$ as Single-Source CVD Precursors for WN_xC_y Thin Films. Correlation of Precursor Fragmentation to Film Properties. *J. Am. Chem. Soc.* **2005**, *127* (21), 7825–7833.
- (80) Cantrell, G. K.; Meyer, T. Y. Transition-Metal-Catalyzed Imine Metathesis. *Organometallics* **1997**, *16* (25), 5381–5383.
- (81) Cantrell, G. K.; Meyer, T. Y. Azaheteroalkene Metathesis: Reaction of Imines with Molybdenum(VI) Bis(Imide) Complexes. *Chem. Commun.* **1997**, No. 16, 1551–1552.
- (82) Cantrell, G. K.; Meyer, T. Y. Catalytic C=N Bond Formation by Metal-Imide-Mediated Imine Metathesis. *J. Am. Chem. Soc.* **1998**, *120* (32), 8035–8042.

- (83) Amato, C. C.; Hudson, J. B.; Interrante, L. V. Gas Phase Decomposition of an Organometallic Chemical Vapor Deposition Precursor to AlN:[Al(CH₃)₂NH₂]₃. *MRS Proc.* **1989**, *168* (1), 119.
- (84) Lewkebandara, T. S.; Sheridan, P. H.; Heeg, M. J.; Rheingold, A. L.; Winter, C. H. Terminal and Bridging Imido Complexes from Titanium Tetrachloride and Primary Amines. Implications for the Chemical Vapor Deposition of Titanium Nitride Films. *Inorg. Chem.* **1994**, *33* (25), 5879–5889.
- (85) Haase, T.; Bahlawane, N.; Strong, J. T.; Jakob, A.; Shen, Y.; Lang, H.; Kohse-Hoeninghaus, K. Mass Spectrometry as a Basis for the Selection of CVD Precursors. *Proc. - Electrochem. Soc.* **2005**, *2005-09*, 276–283.
- (86) Lewis, R. A.; Wu, G.; Hayton, T. W. Stabilizing High-Valent Metal Ions with a Ketimide Ligand Set: Synthesis of Mn(N=CtBu₂)₄. *Inorg. Chem.* **2011**, *50* (10), 4660–4668.
- (87) Lewis, R. A.; Smiles, D. E.; Darmon, J. M.; Stieber, S. C. E.; Wu, G.; Hayton, T. W. Reactivity and Mössbauer Spectroscopic Characterization of an Fe(IV) Ketimide Complex and Reinvestigation of an Fe(IV) Norbornyl Complex. *Inorg. Chem.* **2013**, *52* (14), 8218–8227.
- (88) Neese, F.; Wennmohs, F.; Becker, U.; Riplinger, C. The ORCA Quantum Chemistry Program Package. *J. Chem. Phys.* **2020**, *152* (22).
- (89) Grimme, S.; Hansen, A.; Ehlert, S.; Mewes, J. M. R2SCAN-3c: A “Swiss Army Knife” Composite Electronic-Structure Method. *J. Chem. Phys.* **2021**, *154* (6).

- (90) Ásgeirsson, V.; Birgisson, B. O.; Bjornsson, R.; Becker, U.; Neese, F.; Riplinger, C.; Jónsson, H. Nudged Elastic Band Method for Molecular Reactions Using Energy-Weighted Springs Combined with Eigenvector Following. *J. Chem. Theory Comput.* **2021**, *17* (8), 4929–4945.
- (91) Riplinger, C.; Sandhoefer, B.; Hansen, A.; Neese, F. Natural Triple Excitations in Local Coupled Cluster Calculations with Pair Natural Orbitals. *J. Chem. Phys.* **2013**, *139* (13), 134101.
- (92) Liakos, D. G.; Guo, Y.; Neese, F. Comprehensive Benchmark Results for the Domain Based Local Pair Natural Orbital Coupled Cluster Method (DLPNO-CCSD(T)) for Closed- and Open-Shell Systems. *J. Phys. Chem. A* **2020**, *124* (1), 90–100.
- (93) Addison, A. W.; Rao, T. N.; Reedijk, J.; van Rijn, J.; Verschoor, G. C. Synthesis, Structure, and Spectroscopic Properties of Copper(II) Compounds Containing Nitrogen–Sulphur Donor Ligands; the Crystal and Molecular Structure of Aqua[1,7-Bis(N-Methylbenzimidazol-2'-yl)-2,6-dithiaheptane]Copper(II) Pe. *J. Chem. Soc., Dalt. Trans.* **1984**, No. 7, 1349–1356.
- (94) Fox, H. H.; Yap, K. B.; Robbins, J.; Cai, S.; Schrock, R. R. Simple-High Yield Syntheses of Molybdenum(VI) Bis(IMIDO) Complexes of the Type $\text{Mo}(\text{NR})_2\text{Cl}_2(1, 2\text{-Dimethoxyethane})$. *Inorg. Chem.* **1992**, *31* (11), 2287–2289.
- (95) Kim, S. B.; Sinsermsuksakul, P.; Hock, A. S.; Pike, R. D.; Gordon, R. G. Synthesis of N-Heterocyclic Stannylene (Sn(II)) and Germylene (Ge(II)) and a Sn(II) Amidinate and Their Application as Precursors for Atomic Layer Deposition. *Chem. Mater.* **2014**, *26* (10), 3065–

3073.

- (96) Dyer, P. W.; Gibson, V. C.; Howard, J. A. K.; Whittle, B.; Wilson, C. Four Coordinate Bis(Imido) Alkene Complexes of Molybdenum(IV): Relatives of the Zirconocene Family. *J. Chem. Soc., Chem. Commun.* **1992**, 04 (22), 1666–1668.
- (97) Rosenfeld, D. C.; Wolczanski, P. T.; Barakat, K. A.; Buda, C.; Cundari, T. R.; Schroeder, F. C.; Lobkovsky, E. B. Synthesis and Reactivity of [(Silox)₂Mo=NR]₂Hg (R = TBu, TAmly; Silox = OSitBu₃): Unusual Thermal Stability and Ready Nucleophilic Cleavage Rationalized by Electronic Factors. *Inorg. Chem.* **2007**, 46 (23), 9715–9735.
- (98) Siemeling, U.; Kölling, L.; Kuhnert, O.; Neumann, B.; Stammer, A.; Stammer, H. G.; Fink, G.; Kaminski, E.; Kiefer, A.; Schrock, R. R. Transition Metal Complexes Containing Functionalized Organoimido and Phosphaneiminato Ligands. *Zeitschrift für Anorg. und Allg. Chemie* **2003**, 629 (5), 781–792.
- (99) Dyer, P. W.; Gibson, V. C.; Howard, J. A. K.; Whittle, B.; Wilson, C. Four Coordinate Molybdenum Alkene and Alkyne Complexes Bearing Ancillary Imido Ligands. *Polyhedron* **1995**, 14 (1), 103–111.
- (100) Ruffanov, K. A.; Zarubin, D. N.; Ustynyuk, N. A.; Gourevitch, D. N.; Sundermeyer, J.; Churakov, A. V.; Howard, J. A. K. Synthesis and Structure of a Series of New Haloaryl Imido Complexes of Molybdenum. *Polyhedron* **2001**, 20 (5), 379–385.
- (101) Price, D. M. Vapor Pressure Determination by Thermogravimetry. *Thermochim. Acta* **2001**, 367–368 (June 2000), 253–262.

- (102) Price, D. M. A Fit of the Vapours. *Thermochim. Acta* **2015**, *622*, 44–50.
- (103) Farrugia, L. J. WinGX and ORTEP for Windows : An Update. *J. Appl. Crystallogr.* **2012**, *45* (4), 849–854.
- (104) Neese, F. Software Update: The <sc>ORCA</Sc> Program System—Version 5.0. *WIREs Comput. Mol. Sci.* **2022**, No. November 2021, 1–15.
- (105) Hanwell, M. D.; Curtis, D. E.; Lonie, D. C.; Vandermeersch, T.; Zurek, E.; Hutchison, G. R. Avogadro: An Advanced Semantic Chemical Editor, Visualization, and Analysis Platform. *J. Cheminform.* **2012**, *4* (1), 17.
- (106) Ehlert, S.; Huniar, U.; Ning, J.; Furness, J. W.; Sun, J.; Kaplan, A. D.; Perdew, J. P.; Brandenburg, J. G. R 2 SCAN-D4: Dispersion Corrected Meta-Generalized Gradient Approximation for General Chemical Applications. *J. Chem. Phys.* **2021**, *154* (6), 061101.
- (107) Caldeweyher, E.; Bannwarth, C.; Grimme, S. Extension of the D3 Dispersion Coefficient Model. *J. Chem. Phys.* **2017**, *147* (3), 034112.
- (108) Caldeweyher, E.; Ehlert, S.; Hansen, A.; Neugebauer, H.; Spicher, S.; Bannwarth, C.; Grimme, S. A Generally Applicable Atomic-Charge Dependent London Dispersion Correction. *J. Chem. Phys.* **2019**, *150* (15).
- (109) Kruse, H.; Grimme, S. A Geometrical Correction for the Inter- and Intra-Molecular Basis Set Superposition Error in Hartree-Fock and Density Functional Theory Calculations for Large Systems. *J. Chem. Phys.* **2012**, *136* (15), 154101.
- (110) Zhang, Y.; Yang, W. Comment on “Generalized Gradient Approximation Made Simple.”

- Phys. Rev. Lett.* **1998**, *80* (4), 890–890.
- (111) Grimme, S.; Antony, J.; Ehrlich, S.; Krieg, H. A Consistent and Accurate Ab Initio Parametrization of Density Functional Dispersion Correction (DFT-D) for the 94 Elements H-Pu. *J. Chem. Phys.* **2010**, *132* (15), 154104.
- (112) Allouche, A. Software News and Updates Gabedit — A Graphical User Interface for Computational Chemistry Softwares. *J. Comput. Chem.* **2012**, *32* (Sfb 858), 174–182.
- (113) Weigend, F.; Ahlrichs, R. Balanced Basis Sets of Split Valence, Triple Zeta Valence and Quadruple Zeta Valence Quality for H to Rn: Design and Assessment of Accuracy. *Phys. Chem. Chem. Phys.* **2005**, *7* (18), 3297.
- (114) Andrae, D.; Huzarnermann, U.; Dolg, M.; Stoll, H.; Preußner, H. Energy-Adjusted ab Initio Pseudopotentials for the Second and Third Row Transition Elements. *Theor. Chim. Acta* **1990**, *77* (2), 123–141.
- (115) Hanson, R. M.; Prilusky, J.; Renjian, Z.; Nakane, T.; Sussman, J. L. JSmol and the Next-Generation Web-Based Representation of 3D Molecular Structure as Applied to Proteopedia. *Isr. J. Chem.* **2013**, *53* (3–4), 207–216.
- (116) Pettersen, E. F.; Goddard, T. D.; Huang, C. C.; Couch, G. S.; Greenblatt, D. M.; Meng, E. C.; Ferrin, T. E. UCSF Chimera?A Visualization System for Exploratory Research and Analysis. *J. Comput. Chem.* **2004**, *25* (13), 1605–1612.

For Table of Contents Only

The thermal stability and decomposition of a series of *bis*(alkylimido)-dichloromolybdenum(VI) complexes with various *N,N'*-chelates was investigated. Most of the compounds follow the same decomposition pathway. First, the *N,N'*-chelating ligand dissociates, then the unligated species undergo intramolecular γ -H transfer to another imido ligand, resulting in a *tert*-alkylamido ligand and a nitrido moiety. Ultimately the compounds decompose to yield primary *tert*-alkylamines, alkenes, and β -Mo₂N.

